Available online at www.sciencedirect.com
ScienceDirect
Journal of Power Sources 159 (2006) 758–780
JOURNAL OF POWER SOURCES
www.elsevier.com/locate/jpowsour

POWER (power optimization for wireless energy requirements): A MATLAB based algorithm for design of hybrid energy systems

K.A. Cook [a], F. Albano [b], P.E. Nevius [c], A.M. Sastry [a,b,c,*]

[a] *Department of Biomedical Engineering, University of Michigan, Ann Arbor, MI 48105, USA*
[b] *Department of Material Science Engineering, University of Michigan, Ann Arbor, MI 48105, USA*
[c] *Department of Mechanical Engineering, University of Michigan, Ann Arbor, MI 48105, USA*

Received 12 July 2005; received in revised form 12 October 2005; accepted 17 October 2005
Available online 20 December 2005

Abstract

We have expanded and implemented an algorithm for selecting power supplies into a turnkey MATLAB code, "POWER" (power optimization for wireless energy requirements). Our algorithm uses three approaches to system design, specifying either: (1) a single, aggregate power profile; (2) a power system designed to satisfy several power ranges (micro-, milli- and Watt); or (3) a power system designed to be housed within specified spaces within the system. POWER was verified by conducting two case studies on hearing prosthetics: the TICA (LZ 3001) (Baumann group at the Tübingen University) and Amadeus cochlear implant (CI) (WIMS-ERC at the University of Michigan) based on a volume constraint of 2 cm^3. The most suitable solution identified by POWER for the TICA device came from Approach 1, wherein one secondary cell provided 26,000 cycles of 16 h operation. POWER identified Approach 2 as the solution for the WIMS-ERC Amadeus CI, which consisted of 1 cell for the microWatt power range and 1 cell for the milliWatt range (4.43 cm^3, ~55% higher than the target volume), and provided 3280 cycles of 16 h operation (including re-charge of the batteries). Future work will be focused on continuously improving our present tool.

Keywords: MEMS; Batteries; Hybrid; Algorithm; Cochlear; Implant

1. Introduction

Recently, we introduced an algorithm [1] to design hybrid battery systems for multi-component, wireless microelectronics. Proof of concept was established using the Wireless Integrated Microsystems Engineering Research Center (WIMS-ERC) Environmental Monitor Testbed (EMT) at the University of Michigan. Use of our algorithm resulted in significant reduction in both mass and volume of power supplies, over trial-and-error selection of batteries. For the WIMS-ERC EMT testbed, we designed a power supply weighing 32 mg, comprised of thin-film lithium-free [2] and prismatic lithium polymer secondary cells; these were, respectively, the Ultralife UBC422030/PCM and UBC641730/PCM [3].

Our methodology [1] constrained operating temperature, energy/power density, and specific energy/power; we further allowed requirements/constraints on rechargeability, mass, volume, and lifetime in selection of appropriate battery electrochemistries and configurations (i.e. parallel, series, or combinations thereof). Our algorithm separately evaluated results of three approaches to system design, specifying either: (1) a single, aggregate power profile; (2) a power system designed to satisfy several power ranges (micro-, milli- and Watt); or (3) a power system designed to be housed within specified spaces within the system, with device constraints on volume and surface area.

In this paper, we describe the expansion and implementation of our algorithm into a turnkey MATLAB [4] code. We set out the following objectives in this work, to expand our original algorithm to its present realization:

(1) to implement simple models to account for capacity fade as a function of discharge current and cycling, using our own, and manufacturer-generated data on primary coin cells;
(2) to implement an algorithm for binning device voltage and current requirements within the micro-, milli- and Watt power ranges, along with expressions for calculating tar-

* Corresponding author.
E-mail address: amsastry@umich.edu (A.M. Sastry).

0378-7753/$ – see front matter © 2005 Elsevier B.V. All rights reserved.
doi:10.1016/j.jpowsour.2005.10.062

Nomenclature

Alphabet

a	number of cell configurations (integer number)
b	voltage (V)
c	cycle (integer number)
e	energy (Wh)
I	current (A)
L	lifetime (cycles)
M	mass (kg)
N	number of cells (integer number)
P	percent capacity fade (normalized number in the interval [0,1])
p	power (W)
t	time (s)
V	volume (L)
w	weighted power (W)
X	total capacity (Ah)

Greek symbols

χ	capacity (Ah) at a given time increment

Superscripts and subscripts

c	cycle
ctr	counter
ctr_com	counter
i	index
loc	power site
p	primary
r	rth cell
s	secondary
sys	system
total	summation
$\sim$	specific property (kg^{-1})
$\hat{}$	density (L^{-1})

get micro-, milli- and Watt mass, volume and area target values, based on user-defined battery numbers;

(3) to implement criteria in the algorithm to limit voltage and current of power sites; and finally,

(4) to implement a discretization scheme for user-input current profiles.

This new code, "POWER" (power optimization for wireless energy requirements), employs a graphical user interface (GUI) to allow step-by-step input of system data by the user. To verify our implementation, we conducted two case studies in power selection. The first was a re-examination of work done at Tübingen University [5–8] in a fully implantable hearing prosthesis designed to mechanically stimulate the tympanic membrane, the Totally Implantable Communication Assistance (TICA) [5–8]. The second case study comprised design of a power system for a novel cochlear implant, the Amadeus, developed at the University of Michigan's WIMS-ERC [9–11].

2. Background

2.1. Cell capacity

Theoretical cell capacity is determined as the ratio of the sum of the electrochemical equivalent of the active materials, and the total number of electrons involved in the reaction. Capacity fade, i.e. loss of discharge capacity when the battery is inactive ("calendar life" loss) or in use ("cycle life" loss), can substantially reduce performance [12]. This phenomenon has been extensively studied in primary and secondary lithium-silver-vanadium-oxide, lithium-manganese dioxide, lithium-thionyl, zinc-silver oxide; and lithium, lithium-ion, lithium polymer, and zinc silver nickel metal hydride cells, respectively, by the biomedical device [13–15], defense [16], computer [17], hybrid and electrical vehicle [18,19], and cellular phone [20] industries. It can be reversible, in which case it is commonly referred to as self-discharge. Industrially, battery capacity lost in an open-circuit, i.e. where no load is attached to the battery, is also called local action [12,21–23].

Capacity fade is more pronounced at high rates of discharge [24–27], and is further affected by depth of discharge (DOD) [28,29], number of cycles [30–32], materials used (e.g. chemically co-precipitated calcium zincate as an active material in zinc electrodes [33] and Si3-xFexN4 compound as a possible anode for rechargeable lithium batteries [34]), and/or use of additives (e.g. metallic bismuth in zinc electrodes [33], and amorphous manganese oxides [35] and ketjen black dispersed in organic solvents used in lithium-ion cells [36]). High operating temperatures (e.g. for lithium and lithium-ion cells [12,17,30,37,38]) and high storage temperatures (e.g. for lithium-ion batteries [29,38,39]) can also exacerbate capacity fade. Restrictions on operating and storage temperatures have limited use of lithium-ion cells in self-heating portable electronics [17], under moderate and high discharge currents.

2.2. Specific energy/power, power/energy density and rate characterization

Throughout the rest of this paper, we classify ranges of specific power and energy for batteries as shown in Table 1, based on common usage in the literature [40,41]. Table 2(a) (using information from [42]) lists primary electrochemistries intrinsically high in specific energy. Table 2(b) (using information from [16,41–43]) lists secondary electrochemistries intrinsically high in specific power. Batteries presently in the POWER database were selected from the high specific energy/power ranges defined in Table 2(a) and (b).

Table 1
Classification of specific power and energy ranges for primary and secondary cells [16,42,58]

	Specific power ($W\,kg^{-1}$)	Specific energy ($Wh\,kg^{-1}$)
Low	$\tilde{p} < 70$	$\tilde{p} < 40$
Medium	$70 < \tilde{p} < 300$	$40 < \tilde{p} < 80$
High	$\tilde{p} \leq 300$	$\tilde{p} \leq 80$

Table 2
Primary and secondary electrochemistries intrinsically high in specific energy

Anode	Cathode	Electrolyte	Nominal voltage (V)	Cell type	Specific energy ($Wh\,kg^{-1}$)	Energy density ($Wh\,L^{-1}$)	Specific power ($W\,kg^{-1}$)	Operating temperature (°C)
(a) Primary cells								
High specific energy and medium specific power								
Li	So_2	Organic solvent	3.0	Cylindrical	260	415	90	−55–70
Li	MnO_2	Organic solvent	3.0	Button	230	545	65	−20–55
High specific energy and low specific power								
Zn	O_2 (air)	KOH (aqueous)	1.5	Prismatic	370	1300	8	0–50
Zn	O_2 (air)	KOH (aqueous)	1.5	Cylindrical	300	800	8	0–50
Zn	MnO_2	KOH (aqueous)	1.5	Cylindrical	100	195	50	−60–85
Zn	HgO	KOH or NaOH (aqueous)	1.35	Button	100	470	10.5	0–55
(b) Secondary cells								
High specific power and low/medium specific energy								
Pb	PbO_2	H_2SO_4 (aqueous)	2.0	SLI (starting lighting and ignition) prismatic	35	70	1600 (10 s) to 800 kW (0.1 s)[5]	−40–55
MH	NiOOH	KOH (aqueous)	1.2	Button, cylindrical, and prismatic	75	240	2000–2200[2]	−20–50
Zn	NiOOH	KOH (aqueous)	1.65	Cylindrical, prismatic sealed and vented	50–60	80–120	300	−10–50
High specific power and high specific energy								
Zn	MnO_2	KOH (aqueous)	1.5	Cylindrical	85	250	150	−20–40
C	$LiCoO_2$	Organic solvent	4.0	Cylindrical and prismatic	150	400	650[3]	−20–50
Zn	AgO	KOH (aqueous)	1.5	Prismatic	105	180	600[4]	−20–60

Data taken from [16,42,58].

2.3. Strategies employed previously, and present approach

Most power supplies for microelectronic devices are prescribed after design is nearly complete. Power supplies are thus frequently an afterthought: of the microelectronic devices listed in Table 3 [44–49] only one was operated and tested with a battery [45]. All others used external power supplies.

The devices in Table 3 require power in the milliWatt range (0.3–25 mW) and voltages >3.3 V. Indeed, though not evenly-spaced in terms of order-of-magnitude, the ranges of micro-, milli- and Watt power arise commonly in wireless electronics due to the intrinsic demands of their subcomponents. Dynamic power switching, ubiquitous in wireless devices, requires power in the milliWatt range [1], and is required for device activation, volume fluctuation, wireless data transmittal/reception, computation, heating/cooling, actuation, and alarms (Tables 3 and 4). Innovations in the field have resulted in reductions in supply voltage and increases switching frequency [50–52], which in turn have resulted in reductions in milli- and Watt power range consumption. In the milliWatt range, for example, improvements in adiabatic differential switch logic and gate resizing for very large scale integrated (VSLI) circuits have reduced power demands by 26% and 2.8–27.9%, respectively [50,53,54]. In the Watt range, improvement of parallel Huffman decoders, and improvements in first level filtering caches used for modem microprocessors have reduced power demands by 50 and 58%, respectively [54,55]. It must be noted, however, that power reduction frequently comes at the expense of speed of execution, bandwidth, clock speed, and energy delay [1,55]. Thus, further reductions of power in these established ranges will require examination of tradeoffs.

Sample intrinsic specific power/energy, and energy/power densities (which can presently supply power in these ranges at needed rates of discharge) are listed in Appendix A. Most electrochemistries provide nearly constant capacity values for discharge rates within a 35% range, so that binning of power according to power ranges of smaller steps (e.g. every 10 μW) is excessively computationally intensive. Furthermore, power consumption of complimentary metal oxide materials (CMOS) devices, primarily a component of dynamic switching power, is a function of the intrinsic material properties of CMOS materials, namely capacitance due to charge/discharge switching [1]. Thus, the presently-used electrochemistries appear sufficiently robust at this time to power the likely demands of microcircuits, in the near term.

3. Methods

3.1. General methodology and definitions of terms

A flowchart for our algorithm is given in Fig. 1(a) and (b); it is modified to reflect changes from our first work using this approach [1]. The user provides target values for mass, volume, and surface area, operational temperature, numbers of power bundle locations, number of cycles, selection of primary or secondary cells, and mass or volume optimization. We have reduced the number of user inputs in comparison to our past work [1],

Table 3
Typical discharge current requirements for microelectronics [44–49]

Microelectronic device	Technology	Size	Power–current–voltage requirements	Power source
Micro magnetic sensor	Mineral insulated (MI) sensor constructed using CMOS IC multivibrator circuit	Wire diameter = 30 μm, length = 2 mm	0.5–5 mW (pulse current = 30 mA)	External power supply
Colpitts transmitter	Five-turn dielectric suspended inductor was fabricated using a dissolved wafer process	Colpitts oscillator transmitter (5 mm × 5 mm area) each coil is 25 μm wide, 5 μm thick	100 μA with driving voltage = 3.0 V	Operated with 3 V battery
Si-based micro-machined gas sensor	Sensor array was fabricated using a post-process micro-machining technique of standard CMOS process	Thickness = 1.2 μm, active area = 80 μm × 80 μm	9 mW of drive power with 2.0 V drive voltage	External power supply
Amperometric potentiostat	Potentiostat uses an ADC circuit that allos the direct conversion of electrode current in nanoampere range to low-voltage CMOS levels using four operational applifiers	Volume < 3 cm^3	0.65 mW, 260 μA and 2.5 V	3 V lithium coin cell suggested
Electrothermal actuator	MEMS polysilicon surface micromachined electroactuator uses resistive Joule heating to generate expansion and movement	462.5 μm × 15 μm × 129.5 μm	~7–25 mW	External programmable power supply
Three-axial force sensor	Si-based three-axial force sensor to be used in a flexible smart interface for biomechanical measurements	2.3 mm × 2.3 mm × 1.3 mm sensors have implanted piezoresistors that are 6 μm × 30 μm	10–1 mW input voltage = 3.3 V	External power supply

wherein users were required to specify target values for the mass and volume for each power range. Instead, these values are calculated based on the maximum number of cells for each approach specified by the user. Specifically, the target volume, V_i, and mass, M_i, for each power range are computed from the expressions

$$V_i = \frac{N_i}{N_{\text{total}}} V_{\text{sys}} \qquad i = \begin{cases} 1 \text{ for microWatt power range} \\ 2 \text{ for milliWatt power range} \\ 3 \text{ for Watt power range} \end{cases} \tag{1}$$

and

$$M_i = \frac{N_i}{N_{\text{total}}} M_{\text{sys}} \qquad i = \begin{cases} 1 \text{ for microWatt power range} \\ 2 \text{ for milliWatt power range} \\ 3 \text{ for Watt power range} \end{cases} \tag{2}$$

where N_i ($i = 1$, 2, and 3) is the target number of cells for the micro-, milli- and Watt power ranges, respectively, N_{total} is the total number of cells, V_{sys} is the total volume and M_{sys} is the total mass of the desired power supply.

Table 4
Typical discharge current requirements for common commercial electronics [42]

Device	Current drain (mA)		
Cassette recorders	70–130 (low)	90–150 (medium)	100–200 (high)
Disk players		100–350	
Calculators (LCD)		<1	
Cameras	800–1600 (photo flash)	200–300 (autowind)	500–1600 (digital cameras)
Cellular phones		300–800	
Camcorders		700–1000	
Computers	400–800 (palm held)	500–1500 (note book)	800–1000 (laptop)
Fluorescent lamp		500–1000	
Flashlight		100–700	
Memory		0.001	
Remote control		10–60	
Radios: 9 V battery	8–12 (low volume)	10–15 (medium volume)	15–45 (high volume)
Radios: cylindrical battery	10–20 (low volume)	20–30 (medium volume)	30–100 (high volume)
Walkman		200–300	
Smoke detector	0.010–0.015 (background)		10–35 (alarm)
Motorized toys		600–1500	
TV: portable		400–700	

The user defines current and voltage in terms of time increments, prior to entry of device current and voltage values. A duty cycle is the minimum time interval that can be repeated to represent the lifetime usage profile of the device. For a cochlear implant, for example, a typical duty cycle would be a single day, and would include active usage that varied throughout waking hours, with recharging occurring during sleep or off periods. Device current requirements are rarely constant; for example, the current versus time profile for a hearing aid [56] fluctuates over a 60 s period (Fig. 2(a)).

Due to the impracticality of mapping small fluctuations, data can be coarsened for input into POWER using two methods: (1) consolidation of identical current values into the same time interval, or (2) replacement of sufficiently similar current values such that they produce nearly identical values of discharge rate, either with the summed weighted averages of two current magnitudes, or highest of the two current magnitudes; the approach is shown schematically in Fig. 2(b). In the case of the hearing aid current profile shown in Fig. 2(a), fluctuations in current reflect variations in sound volume external to the user [56]. In the plot shown in Fig. 2(b), common currents are combined, for data entry into POWER.

Table 5 gives the relations used in computing of energy e_i, weighted power w_i specific energy (energy per unit target mass) $\tilde{e}_i$, weighted specific power (power per unit target mass) $\tilde{p}_i$, energy density (energy per unit target volume) $\hat{e}_i$, and weighted power density (weighted power per unit volume) $\hat{p}_i$. The nominal voltage of the cell is the operating or rated voltage of the cell specified by the manufacturer.

Devices are classified as having microWatt and milliWatt power ranges, for powers requiring less than one milliWatt, and less than 1 W, respectively. In our previous work [1], this logic was applied iteratively: sub-devices contributing to the largest power values within a particular power range were removed and placed in a higher power range than their initial position, as needed. Here, power ranges not meeting the power range requirements are rearranged according to voltage value. Specifically, devices within a power range are ranked in descending order by operating voltage. Sub-devices contributing the largest voltages within the microWatt or milliWatt power ranges are

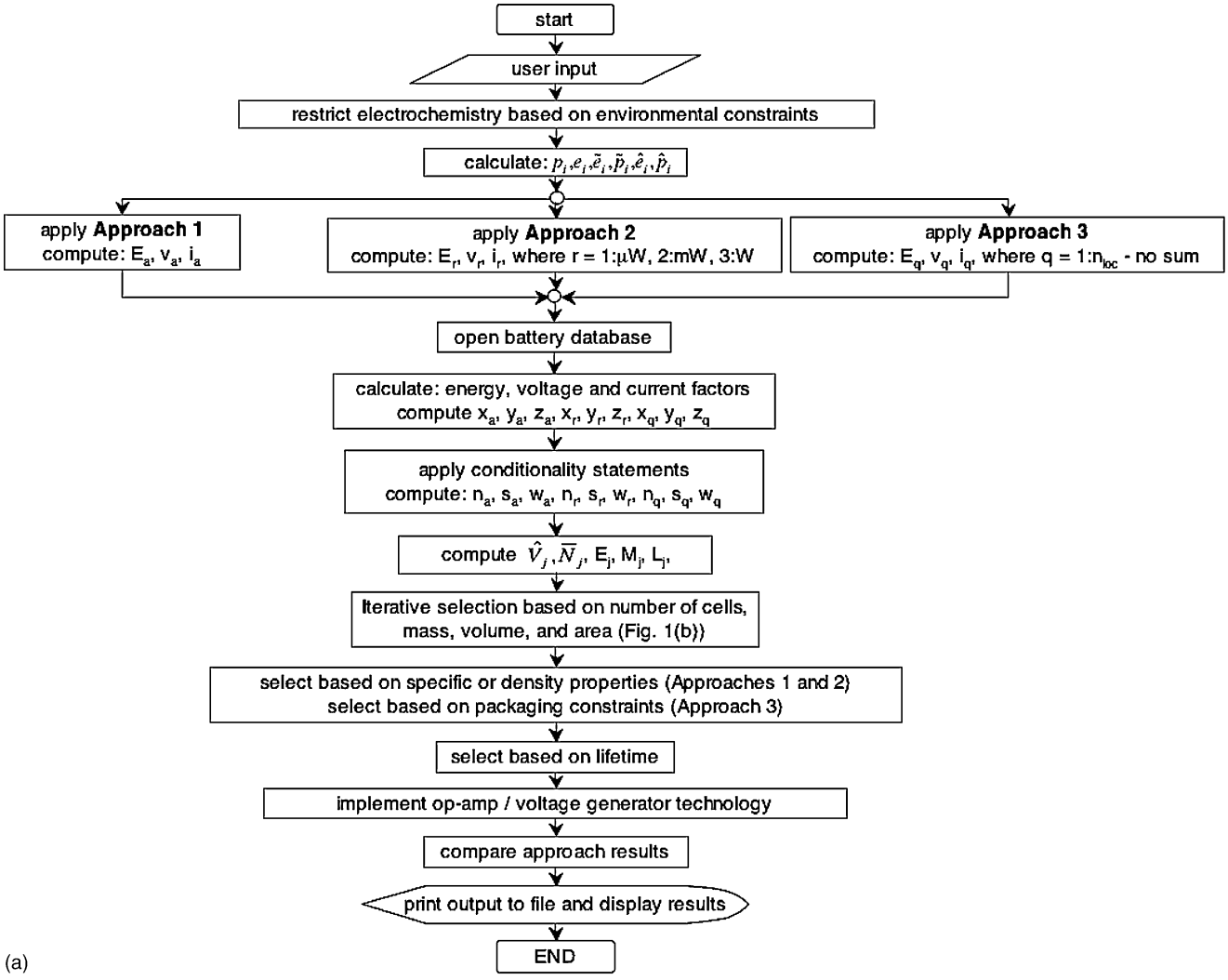

(a)

Fig. 1. [2] Flowchart for logic implemented in POWER. [2] Flowchart for logic used in limiting mass, volume, surface area and number of cells prior to specific energy, energy density and lifetime selection processes.

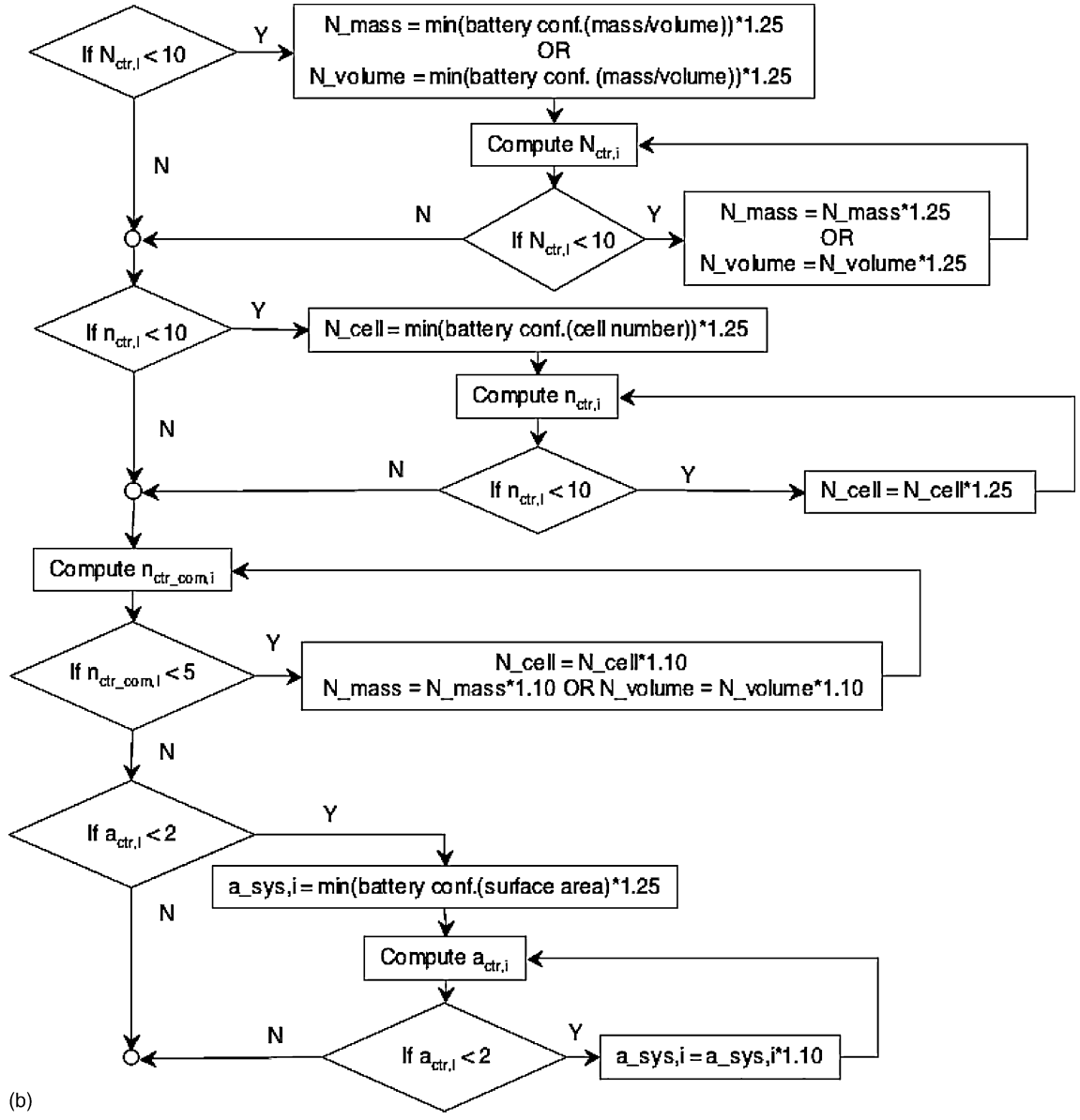

Fig. 1. (*Continued*).

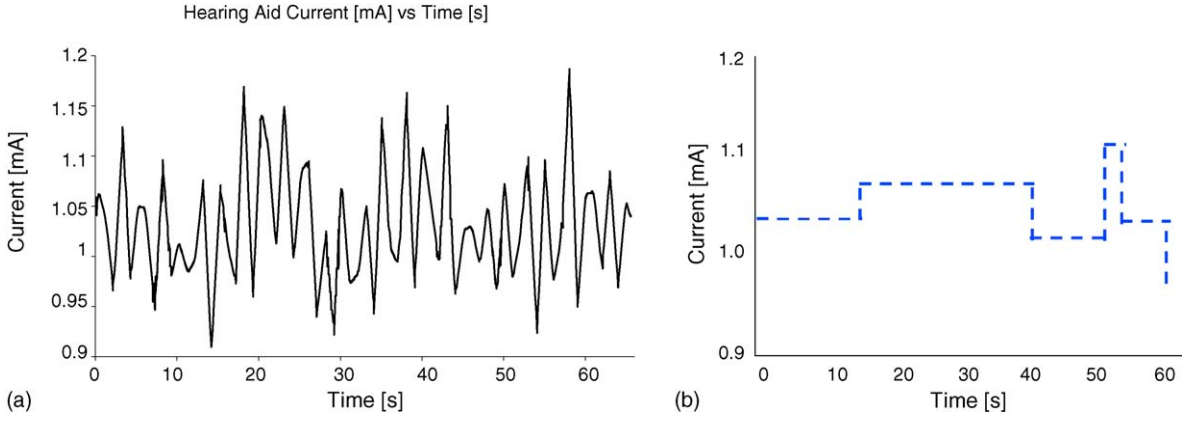

Fig. 2. (a) Current vs. time data for 'Digital Aid X' hearing aid tested by Denis Carpenter of Rayovac [56]. (b) Data after data coarsening, for input into POWER.

Table 5
Relations used in POWER to calculate energy, weighted specific power, specific energy, energy density and weighted power density [1]

Variable	Units	Expression
Power	(W)	$p_i(t) = c_i(t) \times v_i(t), \quad i = 1 : N$, no sum
Energy	(Wh)	$e_i = p_i(t)\Delta t$
Specific energy (for each sub-device)	(Wh kg^{-1})	$\tilde{e}_i = \frac{p_i(t)\Delta t}{m_x}$
Weighted specific power (for each sub-device)	(W kg^{-1})	$\tilde{p}_i = \frac{(\Delta t/t_T)p_i(t)}{m_x}$
Energy density (for each sub-device)	(Wh L^{-1})	$\tilde{e}_i = \frac{\Delta t p_i(t)}{v_x}$
Weighted power density (for each sub-device)	(W L^{-1})	$\tilde{p}_i = \frac{(\Delta t/t_T)p_i(t)}{v_x}$
Energy (for system)	(Wh)	$E_x = \sum_{j=1}^{N} p_j(t)t$
Weighted power (for system)	(W)	$P_x(t) = \sum_{j=1}^{N} p_j(t)\frac{t}{t_T}$
Energy provided by battery	(Wh)	$e_j = \sum_{j=1}^{t_T} b_j C_j \frac{t}{t_T}$
Energy factor	[]	$x_j = \frac{E_x}{e_j}$
Voltage factor	[]	$y_j = \frac{V_x}{b_j}$
Current factor	[]	$z_j = \frac{i_x}{i_j}$

systematically removed from one power range and added to the milliWatt or Watt duty cycle, respectively, until the power limit is reached.

The total capacity required by a device for a duty cycle is given by:

$$X_{\mathrm{E521}} = \sum_{t=1}^{t=t_{\mathrm{total}}} \chi_{E521}(I(t)), \tag{3}$$

or simply the sum of capacity values, χ, for each time increment. The number of cycles provided for a primary or secondary cell without recharge, is:

$$L_{\mathrm{p}} = \frac{XV}{E_{\mathrm{k}}}, \tag{4}$$

where X is the capacity of the cell, multiplied by the cell nominal voltage, V, and E_{k} is the energy required; k refers to the system, power range or site. Capacity losses were also considered, and are discussed separately.

3.2. Selection of database batteries

Silver oxide cells (trivalent silver oxide, zinc/divalent silver oxide and monovalent silver oxide) were included due to their intrinsically high energy density (~530 Wh L^{-1}) in comparison to other primary aqueous electrolyte systems [24]. Because of the inherent instability of trivalent and divalent silver oxide, and the two-step discharge curve in the latter electrochemistry, only the zinc/monovalent silver oxide systems are available commercially. We considered use of zinc-silver oxide primary cells because of their high energy density (~530 Wh L^{-1} [24]), high power density [16] and commercial availability, which make them good candidates for power sources for portable electronics requiring low discharge currents (<1 mA). Though these cells have demonstrated relatively high rate performance in applications where size and mass are key constraints [16], most capacity data provided by manufactures is for very low discharge rates/currents (~0.02 to 0.24 mA [57,58]). Furthermore, many portable electronics and implantable devices, such as defibrillators, require continuous discharge currents between 0.5 and 50 mA [13], which substantially exceed typical discharge currents used by manufacturers in testing, as shown in Table 4.

Lithium manganese and lithium thionyl chloride batteries were also included in our database (e.g. batteries manufactured by Maxell [57] and Renata [58], and Electrochem [59]). Lithium thionyl chloride batteries were chosen because of their intrinsically high specific energies (~275 to 715 Wh kg^{-1}), their high nominal voltage of 3.6 V and their flat discharge profile. These batteries are manufactured in several sizes, ranging from small button cells, to cylindrical and prismatic cells, with reported capacities from 0.4 to 10,000 Ah [24]. Lithium thionyl cells, which use $SOCl_2$ as both cathode and electrolyte solvent, contain a passivation layer over the lithium which inhibits self-discharge. This, in turn, results in long shelf life, but also results in some voltage delay after storage. These cells operate over a wide temperature range, −55 to 70 °C [60]. Lithium manganese dioxide cells, which have a solid cathode, are nonpressurized (in contrast with the soluble cathode lithium cell), and thus do not require hermetic seals. They have lower discharge rates, however, than soluble cathode batteries (including lithium thionyl) and inferior low temperature performance (−20 to 55 °C) compared to lithium thionyl batteries. Their specific energies range from 260 to 500 Wh kg^{-1} [24]. They also range in size, from button to small cylindrical cells.

A detailed list of the batteries selected, along with their characteristics, is found in Appendix A. Inherently, performance tradeoffs must be considered with regard to duty cycle, size and discharge current of the power supply. We specifically examined tradeoffs in capacity fade versus application of low-mass batteries in pulse conditions, given the probable stringent size constraints in implantable devices. For example, wristwatch batteries of very low mass are available, but have not been widely used in pulse applications.

3.3. Determination of voltage and current for each power site location

In our previous work, a method for establishing maximum current and voltage for each power site was not addressed; we have added logic to do so the present version of POWER. Target volumes and surface areas for each power site, are provided by the user. Target voltage parameters supplied by the user are sorted in descending order, and maximum voltages are assigned to power site locations by rank. For example, for a system of four devices, with voltages in Table 6(a) and (b), and allocation for only two power sites, would result in assigned voltages for

Table 6
Sample system of four devices with varying voltages, used to demonstrate allocation of voltage values for power site locations; and the resulting assignment of voltage values for two power site locations, based on the system defined

Device	Voltage (V)	Current (mA)
Device #1	15.0	0.001
Device #2	3.0	2.0
Device #3	5.2	1000
Device #4	6.0	0.25

Power bundle site	Volume (cm^3)	Surface area (cm^2)	Voltage (V)	Current (mA)
1	12.0	60.0	15	750
2	5.0	20.0	6.0	250

power sites 1 and 2, of 15 and 6.0 V, respectively. The energy E_i required by each site is simply the volume fraction of the site multiplied by the total energy of the system. The weighted power required for each site, P_i, is similarly the area fraction of the site multiplied by the total system power. The current for each power site is obtained by multiplying area fraction of the site by the maximum current at that site. Thus, the current for each power site in Table 6 would be 0.75 and 0.25 A for sites having areas of 60 and 20 cm^2, respectively (Table 6). The surface area for each cell in the database refers to the total surface of the cell, and not one specific side or face.

3.4. Estimation of capacity fade, for primary and secondary cells

Capacity fade as a function of both discharge current and cycle number was estimated, where possible, using expressions relating capacity fade as a function of cycle from online battery manufacturer data [3,22,56–59,61]. Data used for the empirical regression lines were inclusive of our experimental data and values obtained from the manufacturer [3,22,56–59,61]. At least four data points (e.g. capacity value as a function of current) were used in each plot.

For example, capacity for an Energizer 521 cell was determined via curve-fit of manufacturer-reported data [61] to be:

$$\chi_{E521} = -2.45\ \ln(I(t)) + 3.26, \tag{5}$$

where I is the discharge current for time increment t. Similar relations were generated for all cases using polynomials (limited to third order), logarithmic or power decay functions to reflect the decay of capacity with increased discharge current [24–27]. Correlation factors of >0.80 were deemed acceptable for implementation. This method of computing capacity fade as a function of discharge current was used for both primary and secondary cells.

Capacity fade as a function of cycle was used only for secondary cells. Percent capacity fade as a function of cycle can be expressed as the ratio of capacity provided by a cell at a certain cycle by the maximum capacity the cell can provide, per

$$P_c = \frac{X(c_i)}{X(c_1)}. \tag{6}$$

The total capacity a cell can provide, including all recharge cycles, is thus:

$$X_R = \sum_{c=1}^{c=\text{total cycles}} P_c X(t) \tag{7}$$

This capacity was used by our algorithm to determine the total number of cycles a particular cell can provide for a specific duty cycle, as:

$$L_S = \frac{X_R}{E_k}. \tag{8}$$

The capacity value computed for non-rechargeable systems was used for the energy factor calculation. Cycle time and recharging of cells is incorporated into POWER via Eqs. (6)–(8) for accurate determination of battery solutions' cycle life. Capacity, $X(t)$, is first computed as a function of discharge current over time, per Eq. (3); total capacity as a function of cycle number is then computed via Eq. (7). P_c drops monotonically with cycle number; available capacity thus also drops monotonically with increasing cycle number.

We also generated our own data on primary (i.e. non-chargeable cells) silver oxide cells to estimate capacity fade. Cells were discharged at currents one and two orders of magnitude above the manufacturer-recommended discharge currents, for two reasons. First, many household appliances and electronics (detailed in Table 4) require discharge currents that exceed operational values provided by many manufacturers [57,58,61]. Second, our algorithm requires additional batteries to meet discharge currents (current factor, x_i) that exceed the maximum discharge current allowed for each battery in the database. In cases where manufacture data are provided for small nominal discharge currents, additional batteries are suggested as a solution, to account for losses due to high rate operation.

Silver oxide primary cells (Table 7) were tested to inform a simple model for the relationship between discharge current and capacity. All cells were subjected to constant continuous resistance discharges, wherein the initial open-circuit voltage was approximately 1.55 V and then end voltage was less than 1.0 V. A schematic of the experimental setup is illustrated in Fig. 3. Voltage per second was recorded for each cell, and the

Table 7
Characteristics of silver oxide cells tested

Manufacturer	Part number	Diameter (mm)	Height (mm)	Mass (g)	Resistances tested (kΩ)
Energizer	337	4.80	1.65	0.13	1.25, 1.50, 1.875
Duracell	D379	5.79	2.15	0.23	1.25, 1.50, 1.875
Maxell	SR516SW	5.80	1.65	0.20	1.25, 1.50, 1.875
Maxell	SR616SW	6.80	1.65	0.30	1.25, 1.50, 1.875
Renata	337	4.80	1.65	0.12	100,6.8, 1.0,0.55
Renata	377	6.80	2.66	0.40	0.55, 1.0,2.5, 6.8, 100
Renata	364	6.80	2.15	0.32	0.55, 1.0,2.5
Renata	317	5.80	1.65	0.18	0.55, 1.0,2.5,6.8
Renata	319	5.80	2.70	0.29	0.55, 1.0,2.5, 6.8
Renata	321	6.80	1.65	0.25	0.55, 1.0,2.5,6.8

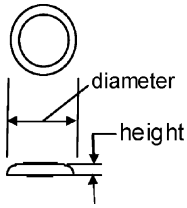

discharge current:

$$I(t) = \frac{b(t)}{R} \tag{9}$$

was determined from the quotient of voltage per unit time, $b(t)$ and resistance, R. The average capacity for each cell was computed as the product of the average current, I_{avg} and total time of operation:

$$C_{avg} = I_{avg} \times t_{total} \tag{10}$$

from an initial voltage of 1.55 V to a cutoff voltage of 1.2 V. Cells were tested at various resistances, to allow curve-fit of a plot of capacity versus discharge current.

3.5. Case studies: fully implantable hearing prosthesis

We selected two fully implantable hearing prostheses as case studies. The first was a mechanical stimulator for the tympanic membrane, the TICA (LZ 3001) device [5–8], designed by researchers at Tübingen University. Specifications on the device's power profile are listed in Table 8.

The second testbed was the WIMS-ERC Amadeus Cochlear Implant [9–11,62,63], developed by researchers at the University of Michigan. Specifications on the device's power profile are listed in Table 9.

3.6. Conditionality statements

Conditionality statements were used to determine configuration of the cells (series, parallel or a combination). Correcting typographical errors in our original work [1], these values are shown as Table 10(a) and (b). Cells can be placed in combinations of series and/or parallel according to energy (x), voltage (y) and current (z) factors (Table 10(a) and (b)). Factors (equations contained in our previous work [1]): x, y and z are ratios of system requirements (energy, voltage and current, respectively) to nominal cell values. Variables, n and s represent the system-required total number of cells, and number of cells in series, respectively. Cells can be placed in parallel to meet discharge current and energy requirements, thus, w and u represent the total numbers of cells placed in parallel, and required to meet energy requirements, respectively.

Factors greater than 1 require additional cells to satisfy energy, voltage and discharge system requirements. For example, for a y of 2, two cells, in parallel, are required to meet the system voltage requirement. Table 10(a) and (b) are circuit diagrams illustrating combinations of cells in series and/or parallel. In some cases, additional cells necessary to meet energy requirements simultaneously result in satisfaction of discharge current requirements, e.g. $z = 5$, $y = 3$ and $x = 2$ (Table 10(b)). Table 10(a) and (b) also contain circuit diagrams illustrating cells in series and/or parallel associated with various combinations of x, y and z values.

After batteries were configured in series or parallel arrangements according to the three approaches, mass, volume, surface area, and number of cells in the configuration were examined. This portion of the algorithm is circled in Fig. 1(a), and expanded with additional detail in Fig. 1(b). These iterative steps (Fig. 1(b)) were implemented to enforce user-defined constraints on maximum number of cells per configuration, surface area and

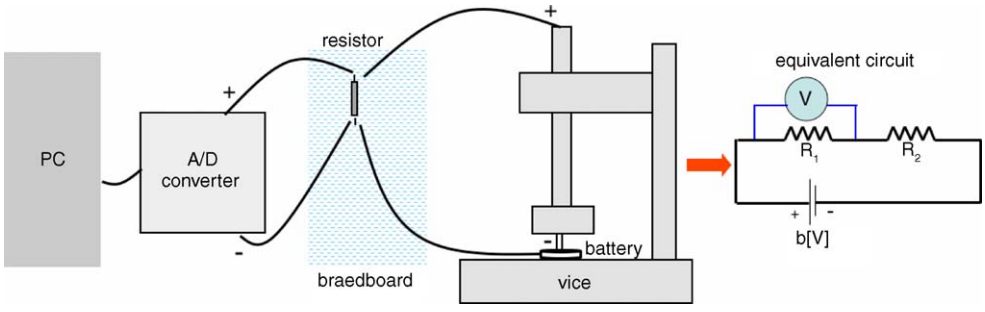

Fig. 3. Experimental setup for resistance testing of primary silver oxide cells.

Table 8
Input parameters for the Tübingen TICA (LZ3001) [5–8] tympanic membrane mechanical stimulator

Electronic components	Input current (mA)	Input voltage (V)	Time interval (s)
Tübingen University—TICA implant—16 h operation			
Microphone	0.05	1.25	60
Signal processor	0.4–0.6	1.25	60
Amplifiers	0.4	1.25	60
Memory (monitoring)	0.1[a]	1.25	60
Signal receiving circuit	0.1	1.25	60
		Total time	16 h
Number of cycles	960	Number of power bundles	2
Surface area of each bundle site	1.0 cm^2	Volume of each power bundle	1.0 cm^3
Total area	2.0 cm^2	Total volume	2.0 cm^3

[a] Value corrected from original reference.

mass (mass prioritization) or volume (volume prioritization), and also to compute the best solutions available, even if they did not meet user requirements.

Table 1(b) schematically shows the methodology by which battery solutions determined based on user-supplied mass or volume prioritization. Specifically, if the number of battery solutions in the database meeting the mass or volume requirements, N_{ctr}, specified by the user is greater than 10, then the number of batteries meeting the minimum requirement for number of cells in the battery solution is determined. So, battery solutions that do not meet the mass or volume requirements are eliminated from the pool of solutions that advance to the next step of analysis. However, if insufficient solutions ($N_{ctr} = 10$) meet the mass or volume requirements, solutions that otherwise would have been eliminated are allowed to advance to the next stages of analysis.

Specifically, the number of configurations within each approach that satisfy the mass (mass prioritization) or volume (volume prioritization) target values are counted ($N_{ctr,r}$ for Approach 1, $N_{ctr,i}$ where $i = 1, 2$ and 3 for micro-, milli- and Watt power ranges; and $N_{ctr,s}$, where $s = 1{:}n\_loc$). If $N_{ctr,i}$ is less than 10, a new target mass or volume is determined from the product of minimum mass/volume of all battery configurations and 1.25. For numbers of configurations that do not adhere to the maximum number of cells, nctr, less than 10, new target values for the maximum number of cells are determined by multiplying the minimum mass/volume of all configurations by 1.25. The code iterates until at least 10 cells meet the mass/volume targets and 10 meet the number of cells per configuration requirements. The number of cells that meet both requirements for mass/volume and number of cells per configuration is determined, N_{nctr_com}. If N_{nctr_com} is less than 5, both mass/volume and maximum number of cells targets values are multiplied by 1.10 and iterated. The number of cell configurations meeting the surface area, actr, is checked and iterated in a similar manner, however, only two cell configurations must meet the surface area requirement (Fig 1(a) and (b)).

3.7. Cost analysis

Although not used as a constraint, we did examine the cost of each power solution generated for the test cases. All specifications for batteries included in the database were readily found online. In some cases, purchase of a large number of cells was required to reduce cost per piece. Appendix A includes battery cell characteristics, e.g. mass, volume, total surface area, electrochemistry, shape and cost for purchases on a per piece basis.

4. Results

4.1. Experimental characterization of capacity fade

Primary silver oxide cells exhibited flat voltage discharge curves and operated at a nominal voltage of 1.55 V, as expected. An example of a discharge at a current of 0.8 mA is shown in Fig. 4 (Maxell 516), with a corresponding plot of curve-fits for capacity as a function of various discharge current shown in Fig. 5. A number of silver oxide cells were subjected to continuous constant resistance loads; in each case, voltage over time was recorded. An expression for the line best fitting the capacity as a function of discharge current was determined and included

Table 9
Input parameters for the WIMS-ERC Amadeus [9–11,62,63] cochlear implant

Electronic components	Input current (mA)	Input voltage (V)	Time interval (s)
WIMS-ERC—Amadeus Cl—16 h operation			
Electrodes	4.10	3.00	60
Microcircuits	0.08	3.00	60
		Total time	16 h
Number of cycles	960	Number of power bundles	2
Surface area of each bundle site	1.0 cm^2	Volume of each power bundle	1.0 cm^3
Total area	2.0 cm^2	Total volume	2.0 cm^3

Table 10
Revised conditionality statements

(a) Condition	Expression	Examples and circuit diagram	x	y	z	n_j	s_j	W_j and U_j
$z<x<y$		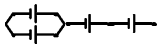	2	3	1	4	3	1 and 2
	$n_j = yz + \|x - z\|$, $s_j = y$, $W_j = z$, $u_j = x$	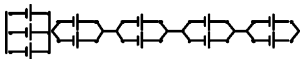	3	5	2	11	5	2 and 3
$x=y>z$		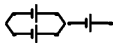	2	2	1	3	2	1 and 2
		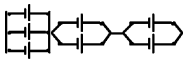	3	3	2	7	3	2 and 3
$y<z<x$ and $y \neq 1$		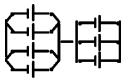	4	2	3	7	2	3 and 4
$z<y<x$		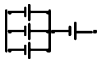	3	2	1	4	2	1 and 3
		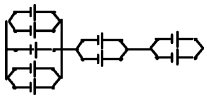	5	3	2	9	3	2 and 5
$y=z<x$ and $y \neq 1$		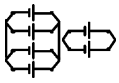	4	2	2	6	2	2 and 4
$y=z<x$ and $y=1$	$n_j = yz + \|x - z\|$, $s_j = y$, $W_j = 0$, $u_j = x$		3	1	1	3	1	0 and 3
$y<z<x$ and $y=1$			3	1	2	3	1	0 and 3

(b) Condition	Expression	Examples and circuit diagram	x	y	z	n_j	s_j	W_j
$x=y=z$			1	1	1	1	0	0
		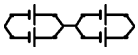	2	2	2	4	2	2
		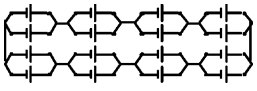	4	4	4	16	4	4
$x<y<z$	$n_j = yz$, $s_j = y$, $W_j = z$		1	2	3	6	2	3
		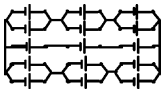	2	3	5	15	3	5
$y<x<z$			2	1	3	3	1	3
		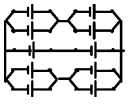	3	2	5	10	2	5
$x<z<y$			1	3	2	6	3	2
		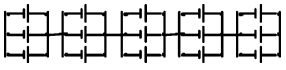	1	5	3	15	5	3
$x=y<z$			1	1	2	2	1	2
		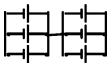	2	2	3	6	2	3

Table 10 (*Continued*)

(b) Condition	Expression	Examples and circuit diagram	x	y	z	n_j	s_j	W_j
$x=z<y$			1	2	1	2	1	2
			2	4	2	8	4	2
$x=z>y$			2	1	2	2	1	2
			3	2	3	6	2	3
$y=z>x$			1	2	2	4	2	2
			2	4	4	16	4	4

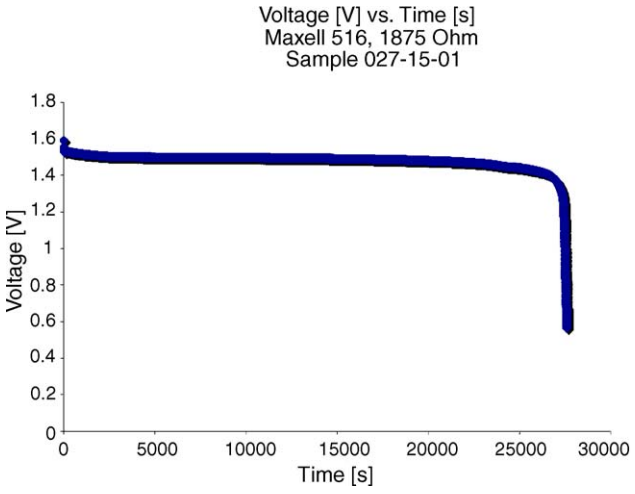

Fig. 4. Voltage vs. time curve obtained from constant resistance testing of a Maxell 516SW silver oxide cell.

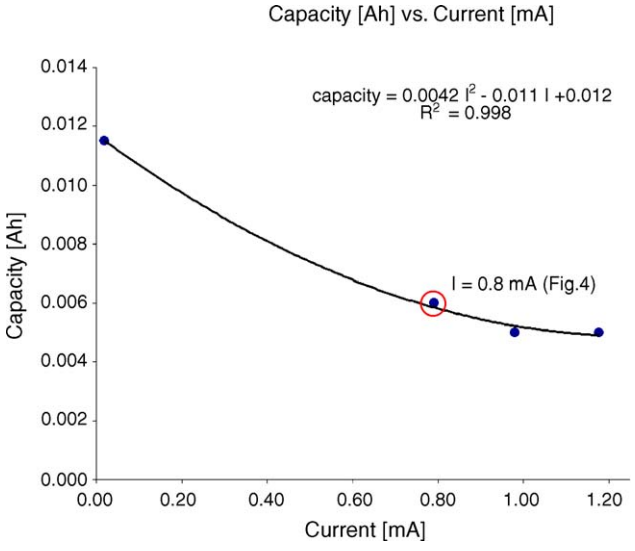

Fig. 5. Sample empirical fit of capacity as a function of discharge current for the Maxell 516SW silver oxide cell.

in our code. Table 11(a) and (b) provide the expression found for each battery tested.

4.2. TICA (LZ 3001) device: 16-h duty cycle

Results for the 16-h operation of the TICA (LZ 3001) device are shown in Table 12. The first of the two tables show the best secondary power solutions. Identical results were obtained for the mass and volume prioritization. Application of Approach 1 resulted in a system comprised of a single cell, the Quallion QL0170E, with a mass of 6.0 g and a volume of 2.62 cm^3. The lifetimes, in terms of cycle number, were calculated to be ∼28 and 25,800, for use of the cell as a primary and secondary source, respectively.

Application of Approach 2 resulted in selection of two Quallion-QL0170E cells (6.0 g and 2.62 cm^3 per cell), one for the micro power range and one for the milli power range, resulting in a total system size of 12 g and 5.24 cm^3. The lifetimes, in terms of cycle number, for both micro- and milliWatt power ranges were 53,700 and 49,600, respectively, when recharge cycles were included.

Using Approach 3, two Quallion-QL0170E cells were selected (6.0 g and 2.62 cm^3), one for each power site, resulting in a total mass and volume of 12 g and 5.24 cm^3. The lifetimes, in terms of cycle number, were both 51,640 for each power site, assuming recharge, i.e. use of the batteries as secondary sources. When volume was selected as the priority, all the three Approaches provided the same results as those determined for the mass priority case.

For comparative purposes, we also used our algorithm to determine the best systems for primary power supplies. One Renata 380 cell was selected for Approach 1 and two Renata 377 cells were selected for Approach 3, one in each available power site. Identical solutions were obtained for both mass and volume prioritization. For Approach 2, mass prioritization resulted in selection of a lighter cell for the microWatt range (Duracell D377, mass equal to 0.4 g); a Renata 380 (1.2 g) cell was selected for volume prioritization. For the milliWatt power range, one Renata 380 cell was selected for both mass and volume priori-

Table 11
Empirically-determined capacity vs. discharge current, for several silver oxide cells tested

Manufacturer	Part number	Resistance (kΩ)	Capacity (mAh)	Current (mA)	Expression
(a)					
Energizer	337	1.25 1.50 1.88	1.01 1.99 2.17	1.13 0.95 0.78	Capacity = $2870I^2 - 8.9I + 0.008$, $R^2 = 0.99$
Maxell	SR516SW	1.25 1.50 188	5.00 5.00 6.00	1.18 0.98 0.79	Capacity = $4228I^2 - 10.77I + 0.012$, $R^2 = 0.99$
Maxell	SR616SW	1.25 1.50 1.88	6.78 6.96 8.45	1.18 0.99 0.80	Capacity = $3854I^2 - 11.84I + 0.015$ $R^2 = 0.99$
Duracell	D379	1.25 1.50 1.88	0.13 1.10 1.26	1.03 0.89 0.71	Capacity = $14200I^2 - 28.37I + 0.015$, $R^2 = 0.99$
Renata	315	0.55 1.00 2.50	7.83 9.72 16.9	2.63 1.47 0.60	Capacity = $1359I^2 - 8.28I + 0.02$, $R^2 = 0.96$
Renata	317	0.55 1.00 2.50 6.80	1.58 2.37 3.64 6.15	2.46 1.43 0.60 0.22	Capacity = $-0.002 \ln(I) - 0.009$, $R^2 = 0.99$
(b)					
Renata	319	0.55 1.00	2.68 4.48	2.53 1.44	Capacity = $-0.004 \ln(I) - 0.02$, $R^2 = 0.99$
Renata	321	0.55 1.00 2.50	1.18 1.28 3.22	2.53 1.43 0.60	Capacity = $0.0001I^{-05}$, $R^2 = 0.97$
Renata	337	0.55 1.00 6.80	1.89 2.54 6.83	2.52 1.36 0.22	Capacity = $1398I^2 - 6I + 0.008$, $R^2 = 1.0$
Renata	364	0.55 1.00 2.50	0.33 0.49 0.62	2.58 1.45 0.60	Capacity = $10^{-6}I^{-09}$, $R^2 = 0.97$
Renata	377	0.55 1.00 2.00 6.80	1.78 4.59 1.23 12.90	2.60 1.43 0.75 0.23	Capacity = $0.02e^{-995}$, $R^2 = 0.95$
Renata	397	0.55 1.00 2.50	14.0 18.50 26.90	2.63 1.48 0.61	Capacity = $0.032e^{-328}$, $R^2 = 0.99$

tization. The cycle life resulting from application of Approach 1 was 5.08; each cycle was 16 h in length, resulting in a total life of just over 3 days. The solution resulting from application of Approach 2 for the microWatt range, provided 3110 cycles of 16 h (∼5.66 years) for mass prioritization and 10,200 cycles of 16 h (∼ 22 years) for volume prioritization. For the milliWatt power range, a lifetime of 9.78 cycles (∼6.7 days) was computed for both mass and volume prioritization. Approach 3 provided a lifetime of approximately 4.4 cycles for both prioritizations.

4.3. WIMS-ERC Amadeus CI: 16-h operation

Results for a 16-h duty cycle for the Amadeus CI are given in Table 13 (secondary cells). When mass was prioritized, application of Approach 1 provided a solution consisting of a single cell, the Quallion QL0170E, of size 6.0 g and 2.62 cm^3. The number of cycles predicted was 3.51, without recharge and 3210, with recharge. Application of Approach 2 resulted in selection of two cells, one Quallion-QL0100E cell (with a mass of 4.0 g and volume of 1.81 cm^3) for the microWatt range, and one Quallion-QL0170E cell (with a mass of 6.0 g and volume of 2.62 cm^3) for the milliWatt range; the total mass and volume of the system were 10 g and 4.43 cm^3, respectively. The calculated lifetime for the battery selected in the microWatt range was 105 cycles as a primary source, and 96,400 as a secondary source. Application of Approach 3 resulted in selection of two Ultralife-UBC641730 cells, one for each power site, resulting in a total mass and volume of 9.0 g and 4.46 cm^3. In this last case, we cal-

Table 12
Binning of devices

Range	Device	Power (mW)	Voltage (V)
(a): Binning of devices into micro and milliWatt power ranges, before any re-arrangement			
Microwatt	1	0.006	1.5
	2	0.950	2.0
	3	0.750	7.0
Total		1.71	
Milliwatt	4	1.5	15.0
	5	2.5	16.0
Total		4.0	
(b): Initial binning of devices within power ranges for a sample system according to power value			
Microwatt	1	0.006	1.5
	3	0.750	7.0
Total		0.756	
Milliwatt	4	1.50	15.0
	5	2.50	16.0
	2	0.95	2.0
Total		4.95	
(c): Final binning of devices within power ranges, for a sample system, according to voltage value			
Microwatt	1	0.006	1.5
	2	0.950	2.0
Total		0.956	
Milliwatt	4	1.50	15.0
	5	2.50	16.0
	3	0.750	7.0
Total		4.75	

culated a lifetime of 7.34 cycles without recharge, and 3200 with recharge.

When primary cells were examined for both mass and volume prioritization computations, the same batteries were selected with application of Approaches 1 and 3. Three cells (Renata 380) were selected for Approach 1 and six cells (Renata 377) were selected for Approach 3, i.e. three per power bundle. For Approach 2 in the microWatt range, one Renata CR2032 (2.8 g) cell was selected in the case of mass prioritization and a Renata CN2450N (5.9 g) cell was selected for volume prioritization. For the milliWatt power range, three Renata 380 cells were selected. The cycle lifetime provided by Approach 1 was 1.9 cycles of 16 h each (∼1.5 days). The system designed by application of Approach 2 for the microWatt range, provided 173,000 cycles for mass prioritization and 712,000 cycles for volume prioritization. For the milliWatt power range, calculated lifetime as 1.9 cycles (∼1.5 day) for both mass and volume prioritization. Approach 3 provided a cycle lifetime of 1.65 cycles (∼1 day) for both prioritizations.

5. Discussion

We have implemented an algorithm into a turnkey battery selection code, POWER, that can be used to design power supply systems for a wide range of wireless devices. Our extension of our original algorithm [] includes consideration of capacity as a function of discharge current, capacity as a function of cycle number, assembly of devices within power ranges based on voltage rather than power, and battery number limitation based on user input and rechargeability.

Table 13
Solutions generated by POWER for the TICA prosthesis implant (secondary batteries)

	Manufacturer	Part No.	Total No.	No. of cycles (no battery re-charge)	No. of cycles (battery re-charge)	Total mass (g)	Total volume (cm^3)
Tübingen TICA—mass priority—16 h of operation							
Approach 1	Quallion	QL0170E	1	28.10	25800	6.00	2.62
Approach 2							
Micro	Quallion	QL0170E	1	58.60	53700	6.00	2.62
Milli	Quallion	QL0170E	1	54.10	49600	6.00	2.62
Totals			2			**12.00**	5.24
Approach 3							
Site 1	Quallion	QL0170E	1	56.30	51600	6.00	2.62
Site 2	Quallion	QL0170E	1	56.30	51600	6.00	2.62
Totals			2			**12.00**	5.24
Tübingen TICA—volume priority—16 h of operation							
Approach 1	Quallion	QL0170E	1	28.10	25800	6.00	**2.62**
Approach 2							
Micro	Quallion	QL0170E	1	58.60	53700	6.00	2.62
Milli	Quallion	QL0170E	1	54.10	49600	6.00	2.62
Totals			2			12.00	**5.24**
Approach 3							
Site 1	Quallion	QL0170E	1	56.30	51600	6.00	2.62
Site 2	Quallion	QL0170E	1	56.30	51600	6.00	2.62
Totals			2			12.00	**5.24**

5.1. Batteries selected and their efficiency in the cases examined

The flat discharge curves of the zinc/monovalent systems make them ideal for nearly constant voltage electronic applications such as watches, calculators, hearing aids and cameras; typical capacities that range from 5 to 250 mAh [24]. These cells also have demonstrated long storage life, retaining more than 95% of their initial capacity after a one year at room temperature. They also exhibit good low temperature performance, and deliver approximately 70% of their capacity at 0 °C and 35% at −20 °C. Their optimal performance temperature range is from 0 to 55 °C [24]. The open-circuit, nominal and cut-off voltages of zinc-silver oxide cells are 1.5–1.6 V, 1.5 and 1.0 V, respectively [16]. The TICA and Amadeus have maximum discharge current and voltage values of 1.25 and 4.18 mA, 3.0 and 1.25 V, respectively. The discharge currents required by these devices are smaller than majority of the devices listed in Table 4. However, the desired battery cycle lifetimes for the TICA and Amadeus are much longer than desired for majority of the devices listed in Table 4. Thus, in comparison to many other common electronics, our devices require batteries that are high in energy density and specific energy and much less demanding in regards to power density and specific power.

5.2. Key difference in power requirements for implanted and explanted or other systems

Presently, biomedical implants such as neurostimulators, drug pumps and implantable defibrillators require high pulse power and long battery life, wherein steady current discharge range could be 0.5–50 mA, and pulse discharge could be up to several hundred mA [13]. The devices examined here, the TICA and Amadeus, have maximum discharge current and voltage values of 1.25 and 4.18 mA, 3.0 and 1.25 V, respectively, with no noted spikes in the current profile.

Approach 1, a homogeneous power supply system based on the aggregate system profile, provided the best and, interestingly, identical solutions for both the TICA [5–8] and Amadeus (6.0 g, 2.62 cm^3, 1 cell [9–11]) implants in terms of smallest mass, volume and number of cells amongst the three approaches—a Quallion QL0170E, lithium polymer cell (6.0 g, 2.62 cm^3, 1 cell). The optimal solution using the same criteria of mass, volume and number of cells, found for the WIMS-ERC environmental monitor testbed from our previous work [1], however, was obtained from Approach 2, power selection based on division of the power requirements based on power ranges of micro-, milli- and Watt power. In this work, a hybrid solution consisting of a thin-film lithium-free cell, 2 Ultralife UBC64130/PCM lithium-ion cells and 5 Ultralife UBC422030/PCM lithium-ion cells were selected. Approach 1 provides the best solution in terms of mass and volume for the implantable system because there are no current, voltage or power spikes/pulses in the power profile, thus eliminating the gains associated with the use of high power density and specific power materials for pulses and high energy density and specific energy materials for the flat portions of the power curve.

Both the WIMS-ERC cochlear and EMT call for use of either lithium or lithium-ion electrochemistries because they fall within the high specific power and high specific energy power range for secondary batteries (Table 2(b)). However, complications associated with the cycling behavior of secondary cells may make their application in implantable systems problematic. Some workers (e.g. [8]) have identified several areas of risk for the use of lithium-ion, lithium polymer, nickel cadmium and nickel metal hydride; similar problems are associated with lithium iodine cells used in cardiac pacemakers [8]:

1. Cell packaging leaks can result in loss of electrolyte, resulting in corrosion damage of electronics. All cell seals must adhere to the standard MIL STD 883D.
2. Outgassing of oxygen and hydrogen at high rates of discharge, cycling over an extended periods, or charge reversal for certain arrangements of cells, can all lead to pressure buildup and unavoidable deformation of cell housings in these necessarily sealed systems.
3. High discharge rates and cycling for extended periods of time can result in elevated temperatures that can lead to heating of the external housing of the cell, implant and surrounding tissue.

Capacity fade and cell swelling in lithium primary cells due to chemical reaction of the electrodes with the electrolyte and the passivation layer have led workers (e.g. [13]) to propose hybrid primary battery systems of lithium iodine and lithium manganese dioxide cells, to power implantable defibrillators. When secondary cells were examined for our testbed cases, lithium-ion cells were chosen for both the Amadeus and TICA devices and Approach 1 provided the best results for mass (6.0 and 6.0 g) and volume (2.62 and 2.62 cm^3) for both cases, respectively. However, if lifetime is the foremost consideration in battery selection, hybrid solutions clearly offer the best result for TICA device, wherein battery cycle life for Approaches 2 and 3 were twice the number of cycles (for both non-recharge and re-charge scenarios) calculated for the system resulting from application of Approach 1.

This is not the case for the Amadeus device, which is operated at a higher discharge current than the TICA device. Here, the number of duty cycles calculated, when recharging is a factor, is essentially the same for all approaches. The only exception is for the microWatt range, wherein the discharge current is so small (80 μA) that the number of cycles is an order of magnitude higher than for the other cases. The impact of capacity fade as a function of cycle is seen in the solution for the Amadeus, where Approach 3 provides more duty cycles before requiring battery recharge. However, the over number of duty cycles provided by the configuration of two cells is nearly equal to those provided by Approach 1.

We have considered the use of voltage regulators and operational amplifier to adjust for voltage in POWER. A problematic effect of these components is the generation of heat, in implantable applications: in general, tissue can only dissipate temperature gradients of less than 2 °C in the temperature range of 37–41 °C [63]. Self-heating of voltage regulators and

operational amplifiers does not entirely prohibit their use in implantable devices, but does merit further investigation on the limits of their usage.

5.3. Lifetime of power designs for applications studied

There are a number of valid reasons to select primary, versus secondary systems, for implantable applications, even if lifetime is somewhat reduced. Chiefly, recharge of secondary systems exposes the patient to potentially high currents, and introduces other possible system failures. As described in Sections 4.2 and 4.3, the best primary systems had significantly reduced lifetime over the best secondary systems examined here (i.e. 28/25,800 and 1.65/3210 battery cycles, for primary/secondary systems, respectively, for the TICA (3001) and WIMS-ERC when subjected to 16 h of operation). But the continuous development of new primary power sources, along with diminishing power demands in microcircuitry, may ultimately make primary systems more attractive.

For the longer lifetime, hybrid secondary systems, a weak-link lifetime was reported, i.e. the lifetime of the shortest lived power supply was reported as the system lifetime. This may be rather overly conservative, since loss of low- or midrange power might be reasonably compensated for by on-board circuitry shunting to the high power system. In any event, a logical and necessary step in hybrid systems is to develop a protocol for warning systems on essential and nonessential power, so that continuous diagnostics can be run in these life-preserving devices.

We also examined limitations on lifetime due to capacity losses, which in turn are linked to operating conditions. In batteries, the level of acceptable irreversible capacity loss (ICL) greater than 20% over a 1–2 year period is generally considered tolerable in portable electronic device batteries, e.g. personal computers and cellular phones [12], but a satellite battery must often retain 80% of its initial capacity for 18 years or more [12]. In the case of implantable systems, the rate of battery capacity fade as a function of cycle has not, to our knowledge, been previously examined. However, implantable devices that prevent and/or limit life threatening physical malfunction require higher standards for battery capacity fade than devices, such as the ones we have studied here, where failure of the devices is not necessarily life threatening.

Low discharge currents allow for optimal capacity from high energy density cells. Approaches 2 and 3 provided superior systems for the implantable devices, in terms of cycle life. In the case of the TICA device, systems designed using Approaches 2 and 3 required more cells, two QL0170E cells, resulting in ∼50,000 duty cycles (including re-charge cycles). Approach 2 provides the best solution for the Amadeus device in terms of battery lifetime (∼96,400 cycles for microWatt and 3280 cycles for the milliWatt power ranges, respectively). So, although Approach 2 does not provide the optimal solution in terms of the mass and volume for the implantable systems, gains in battery cycle life can be achieved with this technique. Since the power profiles for both implants were small in comparison (65–750 μW [TICA] and 0.24–12.3 mW [Amadeus]) to the WIMS-ERC-EMT (18 μW to 3.69 W), the key design factor for the fully implantable system is battery cycle lifetime. Approaches 2 and 3 provide higher battery cycle lives because the power requirements are divided amongst power ranges (Approach 2) or power sites (Approach 3). These implantable devices have discharge current requirements that are small in comparison to many electronic appliances, which generally require several hundred milliWatts for operation (Table 4).

5.4. Effect of capacity loss profiles on selection of power elements

Though generally, a nonlinear relationship between capacity and discharge current is expected [64,42]. Some work has been done to interrogate this relationship in specific systems; for example, nonlinear degradation of capacity as a function of discharge current in zinc-silver oxide cells appears to result from reduced theoretical voltage and side reactions [65]. However, at present, there is insufficient support from a broad range of electrochemical studies to support use of a single model.

Thus, in this present work, we considered polynomial, logarithmic and exponential fits to best fit experimental data, obtained from our experiments and manufacturers' published data. The expressions are applicable within specific discharge ranges noted in Table 11, and we state emphatically that these relationships are not meant to be used to extrapolate behavior outside of the bounds directly tested.

Consideration of capacity as a function of discharge current allowed for inclusion of batteries that would have otherwise been eliminated, if only high capacity values at very low discharge rates provided by manufacturers were considered. For example, Energizer suggests a nominal battery load of 100 kΩ for operation of cell 337 [61]; we demonstrated that these cells can operate at loads up to several magnitudes lower, e.g. 1.25 kΩ (Table 11(a) and (b)). Thus, this battery can be considered for applications where it would have otherwise either been eliminated (from selection based on a 100 kΩ requirement), or in a case wherein a larger number of batteries was suggested, i.e. 100 cells, to meet a higher load.

Batteries were tested at lower discharge resistance values than suggested by the manufacturer, to determine capacity versus discharge currents, at high currents. Cell fabrication and use of additives [66,67] both play key roles in cell capacity, as shown by the data in Table 11; cells having nearly identical shape can exhibit very different capacities, e.g. Energizer versus Renata 337 cells. Other important factors affecting capacity include storage time and temperature; as with any commercial cell, these conditions cannot be fully known a priori, and thus cannot presently be modeled.

Consideration of capacity fade as a function of both cycle number and discharge current can provide a better estimate of battery cycle life. POWER calculates the fraction of capacity provided by a cell with each cycle. These values are used to compute the number of battery cycles provided per recharge, where the battery configuration identified by POWER is expected to satisfy at least one duty cycle before recharge.

5.5. Power range device allocations

Currently, POWER transfers devices to higher power ranges in order of descending voltage value, until the power range requirements are satisfied. POWER, does not, however, go through each combination of devices within a power range to determine which configurations result in the minimal number, mass and volume of batteries; thus, though the solution is improved over the original algorithm, it is not necessarily the optimal one. In our prior work [1], power ranges were arranged by first assigning portions of each device power profile into appropriate power ranges, e.g. portions less than or equal to 1 mW were assigned to the microWatt range, those greater than or equal to 1 mW and less than one Watt were allocated to the milliWatt power range. Portions greater than one Watt were assigned to the Watt power range. Arrangement of devices within power ranges according to voltage is effective because binning devices with voltage requirements reduces the number of batteries placed in series or the number of op-amps/voltage generators needed.

5.6. Power site considerations

The current method of assignment based on descending ranking of values led to some moderate system overdesign. For example, suppose a system of five devices having voltage requirements of 17, 16, 3, 1.5 and 1.2 V required two power site locations (Table 12(a)–(c)). According to the current method of voltage assignment, a 17 V would be assigned to site 1 and 16 V would be assigned to site 2, which would require a minimum of five lithium-ion cells for site 1, and five cells for site 2. However, the number of batteries placed in series to accommodate the voltage requirement could be reduced by placing both the 17 and 16 V devices on one site, and the remaining three devices on the other. Clearly, one site could be allocated to high voltage applications and the other could be dedicated to lower voltage application.

Also, the current assigned to each power site by POWER is the product of the surface area ratio (surface area of individual site to the sum of site areas) and maximum required current. If the resulting current is less than current requirements of devices surrounding the site, additional power programming is required to combine current contributions from multiple sites. Obviously, this eliminates the benefits of a 'stand-alone' system. In the cases examined here, the solutions provided by Approach 3 were quite close (in number of cells, mass and volume) to those recommended by Approaches 1 and 2. However, this was not the case for the WIMS-ERC-EMT system, where values of mass and volume were in close range of Approaches 1 and 2, but the number of cells was 3.6 and 8.1 times those for Approaches 1 and 2.

5.7. Masses and volumes of power bundles

Since most manufacturers select power supplies post facto, Approach 3 provides a means for designing to meet specific surface area and volume constraints. The surface area used in POWER, however, is quite conservative, in that the value of surface area recorded in the POWER database is the entire surface area of the battery. Specifically, if the cell is a rectangular prismatic cell, the surface area is the sum of the area of all six faces. This could lead to elimination of some cells that may meet the area constraints on one side.

Table 14
Solutions generated by POWER for the Amadeus cochlear implant (secondary batteries)

	Manufacturer	Part No.	Total No.	No. of cycles (no battery re-charge)	No. of cycles (battery re-charge)	Total mass (g)	Total volume (cm^3)
WIMS—Amadeus (2005)—Cl—mass priority—16 h of operation							
Approach 1	Quallion	QL0170E	1	3.51	3210	6.00	2.62
Approach 2							
Micro	Quallion	QL0100E	1	105.00	96400	4.00	1.81
Milli	Quallion	QL0170E	1	3.57	3280	6.00	2.62
Totals			2			10.00	4.43
Approach 3							
Site 1	Ultralife	UBC641730/PCM/UMC005	1	7.34	3220	4.50	2.23
Site 2	Ultralife	UBC641730/PCM/UMC005	1	7.34	3220	4.50	2.23
Totals			2			9.00	4.46
WIMS—Amadeus (2005)—Cl—volume priority—16 h of operation							
Approach 1	Quallion	QL0170E	1	3.51	3210	6.00	2.62
Approach 2							
Micro	Quallion	QL0100E	1	105.00	96400	4.00	1.81
Milli	Quallion	QL0170E	1	3.57	3280	6.00	2.62
Totals			2			10.00	4.43
Approach 3							
Site 1	Ultralife	UBC641730/PCM/UMC005	1	7.34	3220	4.50	2.23
Site 2	Ultralife	UBC641730/PCM/UMC005	1	7.34	3220	4.50	2.23
Totals			2			9.00	4.46

Table 15
Commercial biomedical devices [68–74]

Implantable device	Medical condition	Description of device	Location of device	Battery type	Battery lifetime	Device volume (cc) and mass (g)
Cardiac pacemaker [64]	Conduction disorders (bradycardia); heart failure	Three parts: pulse generator, one or two pacing leads and a programmer	Pacemaker: implanted under the skin in upper chest, attached to one or two leads, which are placed next to or in the heart muscle	Lithium iodine (primary)	2–10 years	Pulse generator: 8–16.6 cc, 18–37 g, leads: 46–58 cm
Cardiac defibrillator [42]	Ventricular and atrial tachyarrhythmi a and fibrillation	Three parts: defibrillator, one or two pacing leads and a programmer	Defibrillator: implanted under the skin in the upper chest and is attached to one or two leads, which are placed next to or in the heart muscle	Lithium iodine (primary)	5 years	Defibrillator: 34–65 cc, 70–118 g, leads: 65–110 cm
Muscle stimulators [65]	Urinary and faecal incontinence; gastroparesis	Five parts: neurostimulator, programmer, an extension, a lead, and control magnets	Neurostimulator: implanted subcutaneously in the abdomen; lead placed adjacent to sacral nerve and attached to neurostimulator with extension	Lithium iodine (primary)	6–9 years	Stimulator: 34 cc/42 g
Neurological stimulators [66]	Tremor (e.g. due to Parkinson's disease); pain management (lower leg and back)	Fully implanted system: neurostimulator, lead, extension, programmer, patient programmer, control magnet	Battery: implanted or worn externally; neurostimulator: placed under skin in abdomen or chest cavity for Parkinson's; lead: placed near spine for pain and in brain for Parkinson's, extension connects lead and the stimulator. If external system is used, antenna must be placed on skin with adhesive patch to receive stimulation.	External system: 9 V, internal: lithium iodine (primary)	4–6 weeks (9 years)	Pulse generator: 8–16.6 cc, 18–37 g leads: 46–58 cm
Cochlear implants	Hearing disorders	Consist internal and external components	Internal components: implant package implanted in temporal bone behind the ear and electrode array is introduced into inner ear (cochlear and labyrinth); external components: microphone, speech processor, and external cable [67]	AA batteries or specialized lithium-ion batteries	3–5 days	Depends on manufacturer
Monitoring devices	Syncope; seizures	Consist of electrodes on the surface that sense the hearts electrical activity [68]	Recorder: placed in upper chest cavity; activator placed over heart after seizure to save response information	Primary	1 year	8.8 cc
Drug pumps	Pain caused by: cancer and its treatments, injuries, diabetes; (external/internal pumps), - spasticity (intrathecal baclofen pumps)	Drug delivery system to treat pain: implantable pump, intrathecal catheter, external programmer [69]	Pump: placed in abdominal subcutaneous pocket; catheter: inserted into intrathecal space of spine, and tunneled under skin and connected to the pump	Primary	3 years	10–80 cc
Left ventricular assist devices	Heart failure; bridge to transport or recovery	Three components: pump, tube and power pack	Pump device is implanted into the upper part of the abdominal wall; tube from the pump fits into the left ventricle, and another tube extends outside of the body and is attached to a small battery pack worn on a shoulder holster [70]	AC outlet or two 12 V secondary batteries	5–6 h	119.025 cc, 280.66 g

5.8. Extension of mass, volume and area target values

The code currently examines a minimum of 10 cells, e.g. if only one power solution meets the mass target set by the user, an additional nine power configurations are examined to assure that the configuration also best meet the cell number, areal and specific energy requirements. The advantage of finding the minimum values of solution to meet target values of mass and volume (10 cells), minimum number of cells (5 cells) and surface area requirements (2 cells) so that the algorithm does not converge to a solution in one iteration. Thus, some battery configurations that meet the immediate mass or volume target do not necessarily provide the best specific energy or energy density requirements. As the number of batteries in the database increases, the need for increasing the target values in order to have several available solutions should diminish. Selecting from among the 189 primary and 60 secondary cells in the battery database (Appendix A), only 1 cell configuration met the volume constraint and number of cells constraint (2 cm^3 and 1 cell) for the Amadeus, the Ultralife_UBC322030. However, the solution actually provided by POWER, the Quallion QL0170, though slightly higher in volume (2.6 cm^3) provides a higher energy density, of 268 $Wh\,L^{-1}$, than does the Ultralife cell, 223 $Wh\,L^{-1}$.

Use of the total surface area of the cell does appear to eliminate batteries that may be feasible solutions if assembled on a certain face or side. For example, the solution provided by POWER for the Amadeus, was the Quallion, QL0170 lithium polymer cell, with a total surface area of 12.41 cm^2. The target area was multiplied by 1.25 until a minimum of three cells met the new target surface area, since none of the battery configurations met the original target area constraint (1.0 cm^2). This resulted in identification of three that met the volume, number of cells, energy density and new area constraints: the Quallion_QL0110V (1 cell, 0.0026 L, 153.62 $Wh\,L^{-1}$ and 12.41 cm^2), Quallion_QL0100E 1 cell, 0.0018 L, 223.07 $Wh\,L^{-1}$ and 9.34 cm^2) and Quallion_QL0170E (1 cell, 0.0026 L, 268.38 and 0.0026 L). However, a cell that was smaller in volume that did not meet the area constraint was the Ultralife_UBC641730 (1 cell, 0.0022 L, 330.41 $Wh\,L^{-1}$ and 15.08 cm^3). Because the surface area of largest face of the QL0110, QL0100, QL0170 and UBC641730 are 3.28, 1.248, 3.28 and 5.58 cm^2, respectively, none met the surface area target, but all were closer to the target values than the total surface area of the entire cell.

5.9. Use of secondary versus primary cells

Among the primary cells, the most common electrochemistry that our algorithm selected was the zinc-silver oxide; lithium cells were selected only for the microWatt power range.

Secondary cells selected by POWER for the cochlear implant (16-h operation) weigh less (<5 g, per Tables 13 and 14) than some power systems currently used by commercial cochlear implants (Table 15 [68–74]), such as a 23 g alkaline cylindrical cell (Energizer 391-AA [61]). As expected, Approach 2, through at a penalty of slight increases in mass and volume, provided a higher number of cycles than Approach 1, with and without recharge. It can be seen in Tables 13 and 14 that in all cases, there obviously significant increase in the number of cycles when rechargeability is included, but also at low discharge current, for the microWatt power range.

Because the CI operates at a higher voltage than the TICA device (3.0 V versus 1.25 V), the number of cells required for the former case, for all Approaches. Although Approach 3 presents the smallest mass and volume for all approaches, it requires the highest number of cells (six cells in two bundles); its inherently greater complexity makes it somewhat less appealing than the other approaches. The lifetime for all primary solutions was limited to two cycles.

5.10. Cost analysis

From Appendix A, we see that on average, primary cells meeting the design constraints of the testbed are less expensive than secondary cells. Further, most primary cells listed in the database could be purchased readily online, while the secondary cells were often sold by whole sellers, who required purchase of several hundred cells.

6. Conclusions

Based on the volume constraints (2 cm^3) specified by the workers at Tübingen university in Baumann group [5–8] for the TICA (LZ 3001) device, the most suitable power solution would be the one identified by POWER for Approach 1, secondary cells. Consisting of just 1 cell type Quallion QL0170E (2.62 cm^3), this solution had a volume ∼24% higher than the target value, 2 cm^3. As far as the lifetime is concerned, this solution can provide power for 28 cycles of 16 h each, without need to recharge (448 h, i.e. 18.6 days). Our algorithm also accounts for rechargeability and capacity fade as cells are recharged; therefore, the actual lifetime of 26,000 cycles of 16 h, i.e. 416,000 h or ∼48 years of continuous use. This solution provides a lifetime 10 times longer than the Ni–Cd battery pack that was designed in 1998 [6,8] for the TICA device.

For the WIMS-ERC Amadeus CI [9–11], the best solution among the power sources our code identified was the one of Approach 2, secondary cells. Specifically, a cell type Quallion QL0100E was selected to fulfill the power requirements of the microWatt range sub-devices (microcircuits and microprocessors) and a Quallion QL0170E cell for the milliWatt range (electrode array). The calculated lifetime of this system would be 3280 cycles, corresponding to ∼6.7 years of continuous use. Accounting for system shutdown during 8 of 24 h of usage (sleep), the actual lifetime becomes ∼10 years.

The primary power solutions presented in the current study allowed only a few days' operation. Even so, primary cells deserve further investigation as they present some advantages over secondary power sources. Specifically, primary cells do not rely on patient compliance to operate the implant [75]. Further, primary cells exhibit less outgassing than secondary cells, and thus pose fewer safety concerns in that area [17,18].

Employing a larger volume battery may be a tradeoff that would allow higher reliability and safety. For a volume of ~6 cm^3 (corresponding to 200 Renata 337 cells), a lifetime of more than 2 years can be achieved (~500 cycles of 16 h). However, incorporation of 200 cells would certainly increase the probability of failure, which should be weighed in selection of the final design.

7. Future Work

7.1. Evolution of POWER

Currently the POWER battery database of consists of 189 primary and 60 secondary cells. Additional batteries and other types of power supplies should certainly be included, to continuously take advantage of design innovations.

POWER currently calculates recharge cycles by assuming that the cells are only recharged after at least one duty cycle, at 100% depth of discharge. However, batteries often provide better cycle life when they are recharged at higher levels of DOD. Thus, consideration of depth of discharge would potentially allow for less overdesign, and also allow for inclusion of power scavenging, wherein batteries could be charge during periods of low operation or sleep mode, increasing the number of cycles provided by the system.

7.2. New applications

Several workers have proposed the use of hybrid implantable power systems for neurostimulators, drug pumps and defibrillators (all of which generally have power requirements in excess of those required for pace makers) to combat problems generally associated with implantable batteries: lifetime, swelling (volume change), self-heating and capacity fade [13]. Defibrillators use lithium-silver oxovanadium and lithium-manganese-dioxide cells for power, which are operable at relatively high rates of discharge [13]. Lithium iodine cells are commonly used in pacemakers [13,14].

Most pacemakers consist of a pulse generator, pacing leads, and a controller. The pulse generator and controller have intermittent power profiles, which allow for longer battery lifetimes than continuously-discharged devices. However, the solid electrolytes used in lithium technologies may prevent their use in cochlear implants, due to required high discharge currents necessitated by the high internal resistance in such cells.

These devices, along with more recent devices employing telemetry for physiological monitoring, often outside the clinical setting, have created a need for increased discharge current, although not necessarily greater energy capacity [14]. A number of potential power sources have been examined for such applications, including biogalvanic cells [14]. Nuclear batteries such as those using plutonium 238 as a fuel [14] have also been proposed. However, the extreme toxicity of these materials [14] may preclude their use, even under seal.

Other new elements to consider in novel power supplies include containment of potentially harmful outgas by-products, containment of toxic active materials, implementation of specialized power management software, development of circuitry to monitor charge and tight control of discharge to prevent overheating, overcharge and charge reversal in cells. Operationally, change in temperature and volume during operation, and heat generation, must also be considered. Future work will include these, and other considerations, in continuously improving our present tool.

A systematic approach to selection and design of power systems for microelectronics has not, to our knowledge, been previously reported. The novelty of our procedure is that it takes into account mass and volume design constraints set by the user, and user specific energy/power and energy and power density, to provide concrete solutions. POWER is useful because it incorporates all of the steps in power selection based on mass and volume, and provides a rational means for comparison of power systems.

Appendix A

[22,56–59,61]

Manufacturer	Part No.	Capacity (mAh); $X_i(I)$
Renata	CR1927	$X_{CR927} = 7.92I^2 - 10.97I + 34.4$, $R^2 = 0.95$
	CR1025	$X_{CR1025} = -281.77I^2 - 22.46I + 31.8$, $R^2 = 1.0$
	CR1216	$X_{CR1216} = 68.86I^2 - 39.5I + 26.6$, $R^2 = 0.91$
	CR1220	$X_{CR122} = -69.75I^2 - 1.93I + 38.2$, $R^2 = 0.97$
	CR1225	$X_{CR1225} = 4.17I^2 - 8.94I + 48.9$, $R^2 = 0.97$
	CR1616	$X_{CR1616} = -7.12I^2 - 2.33I + 50.2$, $R^2 = 0.86$
	CR1620	$X_{CR1620} = 6.51I^2 - 14.7I + 69.1$, $R^2 = 0.93$
	CR1632	$X_{CR1632} = -1114.6I^3 + 489.4I^2 - 69.5I + 128.3$, $R^2 = 1.0$
	CR2016	$X_{CR2016} = -41.97I^2 - 0.40I + 82.2$, $R^2 = 0.99$
	CR2025	$X_{CR2025} = -1632.7I^3 + 765.5I^2 - 101.0I + 173.9$, $R^2 = 0.99$
	CR2032	$X_{CR2032} = -814.9I^3 + 468.4I^2 - 85.1I + 240.1$, $R^2 = 0.99$
	CR2320	$X_{CR2320} = 8.05I^2 - 12.0I + 152.3$, $R^2 = 0.98$
	CR2325	$X_{CR2325} = -685.68I^3 + 320.2I^2 - 46.0I + 192.7$, $R^2 = 0.96$
	CR2430	$X_{CR2430} = -2.61I^2 - 0.17I + 285.6$, $R^2 = 1.0$
	CR2440N	$X_{CR2440N} = -9.95I^3 + 14.5I^2 - 7.9I + 542.2$, $R^2 = 1.0$
	CR2477N	$X_{CR2477N} = -5.01I^2 - 0.62I + 956.0$, $R^2 = 0.99$

Manufacturer	Part No.	Capacity (mAh); $X_i(I)$
Electrochem	4301	$X_{4301} = -0.045I^2 + 0.32I + 5280.7$, $R^2 = 1.0$
	44230	$X_{44230} = 1.28I^2 - 40.3I + 1775.6$, $R^2 = 1.0$
	3B960	$X_{3B960} = -1.14I^2 + 1.08I + 792.0$, $R^2 = 1.0$
	3B880	$X_{3B880} = 9.28I^2$ - $62.7I + 1006.2$, $R^2 = 1.0$
	3B940	$X_{3B940} = -0.156I^2 - 1.09I + 1900.1$, $R^2 = 1.0$
	4006	$X_{4006} = 60.61I^2 - 56.4I + 63.0$, $R^2 = 1.0$
	4030	$X_{4030} = -26.0\ln(I) + 534.2$, $R^2 = 0.89$
	4161	$X_{4161} = 0.185I^2 - 4.3I + 824.1$, $R^2 = 1.0$
	4260	$X_{4260} = 0.128I^2 - 13.2I + 5619$, $R^2 = 1.0$
	4204	$X_{4204} = 0.014I^2 - 1.4I + 1622.8$, $R^2 = 1.0$
		Capacity [Ah]
Energizer	521	$X_{521} = -2.45\ln(I) + 3.3$, $R^2 = 0.96$
	528	$X_{528} = 3.67I^2 - 11.3I + 9.0$, $R^2 = 1.0$
	539	$X_{539} = 11.02I^2 - 3.48I + 0.29$, $R^2 = 0.98$
	E91	$X_{E91} = 0.42e^{-0.47 \cdot I}$, $R^2 = 0.92$
	E92	$X_{E92} = -0.17\ln(I) + 0.012$, $R^2 = 0.94$

Manufacturer	Capacity (Ah) X_i and capacity ratio [] $P_{c,j}$
Panasonic	$X_{CGR17500} = -0.05I + 0.84$; $R^2 = 1$ $P_{c,CGR17500} = 4 \times 10^{-7}c^2 - 4 \times 10^{-4}c + 0.98$; $R^2 = 0.98$
Panasonic	$X_{CGR18650HG} = +0008I^2 - 0.86I + 1.84$; $R^2 = 1$ $P_{c,CGR18650HG} = 4 \times 10^{-7}c^2 - 4 \times 10^{-4}c + 0.98$; $R^2 = 0.98$
Panasonic	$X_{CGR18650A} = +0.001I^2 - 0.02I + 1.98$; $R^2 = 1$ $P_{c,CGR18650A} = 4 \times 10^{-7}c^2 - 4 \times 10^{-4}c + 0.98$; $R^2 = 0.98$
Panasonic	$X_{CGR18650C} = -0004I^2 - 0.012I + 2.17$; $R^2 = 1$ $P_{c,CGR18650C} = 4 \times 10^{-7}c^2 - 4 \times 10^{-4}c + 0.98$; $R^2 = 0.98$
Panasonic	$X_{CGA523436} = -0.18I^2 + 0.14I + 0.7$; $R^2 = 1$ $P_{c,CGR18650C} = 4 \times 10^{-7}c^2 - 5 \times 10^{-4}c + 0.98$; $R^2 = 0.97$
Panasonic	$X_{CGA523450A} = 0.1I^2 + 0.09I + 0.93$; $R^2 = 1$ $P_{c,CGR523450A} = -5 \times 10^{-9}c^2 - 2 \times 10^{-4}c + 0.99$; $R^2 = 0.98$
Panasonic	$X_{CGA633450A} = -0.0084I^2 - 0.015I + 1.053$; $R^2 = 1$ $P_{c,CGA633450A} = 6 \times 10^{-8}c^2 - 4 \times 10^{-4}c + 0.98$; $R^2 = 0.98$
Panasonic	$X_{CGA103450A} = -0.013I^2 - 0.01I + 1.94$; $R^2 = 1$ $P_{c,CGA633450A} = 6 \times 10^{-8}c^2 - 4 \times 10^{-4}c + 0.98$; $R^2 = 0.98$
Quallion	$P_{c,i} = 5 \times 10^{-6}c^2 - 0.0134c + 100$; $R^2 = 0.99$ i = QL0003l, QL0700l, QL0110V, QL0900V, QL0100E, QL0170E, QL0320E, QL010KA, QL015KA
Ultralife	$X_{UBC422030} = -333.34I^2 - 35I + 149.25$; $R^2 = 1$ $P_{c,UBC422030} = 96.72e^{-00004 \cdot 1}$; $R^2 = 0.98$
Ultralife	$X_{UBC641730} = -250I^2 - 35I + 199$; $R^2 = 1$ $P_{c,UBC641730} = 96.78e^{-00004 \cdot 1}$; $R^2 = 0.98$
Ultralife	$X_{UBC383450} = 11.77I^2 - 33.7I + 604$; $R^2 = 0.99$ $P_{c,UBC36106102} = 0.057I + 96.63$; $R^2 = 0.99$

Battery type	Part number	Approximate cost q = quantity
Lithium polymer rechargeable	UBC641730/PCM/UMC005	$q = 1$, \$12.07 $q = 12$, \$11.110 $q = 24$, \$10.41 $q = 48$, \$9.720
Lithium polymer rechargeable	UBC433475/PCM/UBC001	$q = 1$, \$17.390 $q = 12$, \$16.01 $q = 24$, \$15.010 $q = 48$, \$14.000
Lithium polymer rechargeable	UBC502030/PCM/UBC006	$q = 1$, \$12.350 $q = 12$, \$11.380 $q = 24$, \$10.66 $q = 48$, \$9.950

Battery type	Part number	Approximate cost q = quantity
Lithium polymer rechargeable	UBC322030/PCM/UBC008	$q = 1$, \$10.930 $q = 12$, \$10.06 $q = 24$, \$9.430 $q = 48$, \$8.80

References

[1] K.A. Cook, A.M. Sastry, An algorithm for selection and design of hybrid power supplies for MEMS with a case study of a micro-gas chromatograph system, J. Power Sources 140 (2005) 181–202.

[2] B.J. Neudecker, N.J. Dudney, J.B. Bates, Lithium-free thin-film battery with insitu plated Li anode, J. Electrochem. Soc. 147 (2) (2000) 517–523.

[3] http://www.ulbi.com, accessed June2005.

[4] http://www.mathworks.com/products/, accessed June 2005.

[5] H.P. Zenner, TICA totally implantable system for treatment of high-frequency sensorineural hearing loss, Ear Nose Throat J. 79 (10) (2000) 770–776.

[6] H. Leysieffer, J.W. Baumann, R. Mayer, D. Muller, T. Schon, A. Volz, H.P. Zenner, A completely implantable hearing aid for sensorineural hearing loss: TICA (R) LZ 30/01, Hno 46 (10) (1998) 853–863.

[7] H.P. Zenner, H. Leysieffer, Total implantation of the implex TICA hearing amplifier implant for high-frequency sensorineural hearing loss—the Tübingen University experience, Otolaryngol. Clin. North Am. 34 (2) (2001) 417–447.

[8] J.W. Baumann, H. Leysieffer, Basics of energy supply to completely implantable hearing aids for sensorineural hearing loss, Hno 46 (2) (1998) 121–128.

[9] B.Y. Arcand, P.T. Bhatti, N.V. Butala, J. Wang, C.R. Friedrich, K.D. Wise, Active positioning device for a perimodiolar cochlear electrode array, Microsyst. Technol. 10 (2004) 478–483.

[10] T.E. Bell, K.D. Wise, D.J. Anderson, A flexible electrode array for a cochlear prosthesis, Sens. Actuators A 66 (1998) 63–69.

[11] M. Ghovanloo, K. Najafi, A compact large voltage-compliance high output-impedance programmable current source for implantable microstimulators, IEEE Transact. Biomed. Eng. 52 (1) (2005) 97–105.

[12] R. Spotnitz, Simulation of capacity fade in lithium-ion batteries, J. Power Sources 113 (2003) 72–80.

[13] J. Drews, G. Fehrmann, R. Staub, R. Wolf, Primary batteries for implantable pacemakers and defibrillators, J. Power Sources 97–98 (2001) 747–749.

[14] W. Greatbatch, Implantable power-sources: a review, J. Med. Eng. Technol. 8 (2) (1984) 56–63.

[15] http://www.bbriefings.com/pdf/753/mdev02_p_soykan.pdf, O. Soykan, Power sources for implantable medical devices, Dev. Technol. Appl. Electron. (2002), accessed 30 June 2005.

[16] A.P. Karpinski, S.J. Russell, J.R. Serenyi, J.P. Murphy, Silver based batteries for high power applications, J. Power Sources 91 (2000) 77–82.

[17] H. Maleki, A.K. Shamsuri, Thermal analysis and modeling of a notebook computer battery, J. Power Sources 115 (2003) 131–136.

[18] X.G. Yang, B.Y. Liaw, Charge performance of a commercial nickel metal hydride traction battery system, J. Electrochem. Soc. 148 (9) (2001) A1023–A1028.

[19] U. Köhler, J. Kümpers, M. Ullrich, High performance nickel-metal hydride and lithium-ion batteries, J. Power Sources 105 (2002) 139–144.

[20] E.A. Cuellar, M.E. Manna, R.D. Wise, A.B. Gavrilov, M.J. Bastian, R.M. Brey, J. DeMatteis, Ultralife's polymer electrolyte rechargeable lithium-ion batteries for use in the mobile electronics industry, J. Power Sources 96 (2001) 184–198.

[21] http://www.intellefleet.com/index.php?ShowPage=Glossary, accessed June 2005.

[22] http://www.ebuybatteries.com/battery_knowledge/battery_glossary.asp, accessed June 2005.

[23] http://www.calpoly.edu/~cm/studpage/eking/definitions.htm, accessed June 2005.

[24] R.B. Wright, J.P. Christophersen, C.G. Motloch, J.R. Belt, C.D. Ho, V.S. Battaglia, J.A. Barnes, T.Q. Duong, R.A. Sutula, Power fade resulting from cycle-life testing of advanced technology development program lithium-ion batteries, J. Power Sources 119–121 (2003) 865–869.

[25] H.T. Liu, X. Xia, Z.P. Guo, A novel silver oxide electrode and its charge-discharge performance, J. Appl. Electrochem. 32 (2002) 275–279.

[26] J.A. Jeevarajan, A.F. Rakotondrainibe, A.J. Appleby, F.E. Little, Performance evaluation and materials characterization of some commercial batteries, in: Proceedings of the 193rd ECS Meeting, San Diego, 7 May, 1998, pp. 363–368.

[27] J.P. Fellner, G.J. Loeber, S.S. Sandu, Testing of lithium-ion 18650 cells and characterizing/prediction cell performance, J. Power Sources 81–82 (1999) 867–871.

[28] K. Takahashi, M. Saitoh, N. Asakura, T. Hibino, M. Sano, M. Fujita, K. Kifune, Electrochemical properties of lithium manganese oxides with different surface areas for lithium-ion batteries, J. Power Sources 136 (2004) 115–121.

[29] T. Osaka, S. Nakade, M. Rajamäki, T. Momm, Influence of capacity fading on commercial lithium-ion battery impedance, J. Power Sources 119–121 (2003) 929–933.

[30] J.R. Belt, C.D. Ho, T.J. Miller, M.A. Habib, T.Q. Duong, The effect of temperature on capacity and power in cycled lithium-ion batteries, J. Power Sources 142 (2005) 354–360.

[31] M. Saft, G. Chagnon, T. Faugeras, G. Sarre, P. Morhet, Saft lithium-ion energy and power storage technology, J. Power Sources 80 (1999) 180–189.

[32] L.S. Kanevskii, V.S. Dubasova, Degradation of lithium-ion batteries and how to fight it: a review, Russ. J. Electrochem. 41 (1) (2005) 1–16.

[33] C. Zhang, J.M. Wang, L. Zhang, J.Q. Zhang, C.N. Cao, Study of the performance of secondary alkaline pasted zinc electrodes, J. Appl. Electrochem. 31 (2001) 1049–1054.

[34] C.-H. Doh, N. Kalaiselvi, C.-W. Park, B.S. Jin, S.-I. Moon, M.-S. Yun, Synthesis and electrochemical characterization of novel high capacity $Si_{3-x}Fe_xN_4$ anode for rechargeable lithium batteries, Electrochem. Commun. 6 (2004) 965–968.

[35] J. Yang, T.B. Atwater, J.J. Xu, Improved cycling performance of bismuth-modified amorphous manganese oxides as cathodes for rechargeable lithium batteries, J. Power Sources 1339 (2005) 274–278.

[36] S. Kuroda, N. Tobori, M. Sakura, Y. Sato, Charge–discharge properties of a cathode prepared with ketjen black as the electro-conductive additive in lithium-ion batteries, J. Power Sources (2003) 924–928.

[37] B.A. Johnson, R.E. White, Characterization of commercially available lithium-ion batteries, J. Power sources 70 (1998) 48–54.

[38] B. Markovsky, A. Rodkin, Y.S. Cohen, O. Palchik, E. Levi, D. Aurbach, A.-J. Kim, M. Schmitt, The study of capacity fading processes of Li-ion batteries: major factors that play a role, J. Power Sources 119–121 (2003) 504–510.

[39] K. Araki, N. Sato, Chemical transformation of the electrode surface of Lithium-Ion battery after storing at high temperature, J. Power Sources 124 (2003) 124–132.

[40] M. Broussely, Recent developments on Lithium-ion batteries at SAFT, J. Power Sources 81–82 (1999) 140–143.

[41] R. Gitzendanner, F. Puglia, C. Martin, D. Carmen, E. Jones, S. Eaves, High power and high energy lithium-ion batteries for under-water applications, J. Power Sources 136 (2004) 416–418.

[42] D. Linden, T.B. Reddy, Handbook of Batteries, third ed., McGraw-Hill, New York, 2002.

[43] M. Klein, M. Eskra, R. Plivelich, A.J. Salkind, J. Ockerman, Performance and electrochemical characterization studies of advanced high-power bipolar nickel/metal hydride batteries, J. Power Sources 136 (2004) 317–321.

[44] T. Kanno, K. Mohri, T. Yagi, T. Uchiyama, L.P. Shen, Amorphous wire MI micro sensor using C-MOS IC multivibrator, IEEE Trans. Magn. 33 (5) (1997) 3358–3360.
[45] B. Ziaie, K. Najafi, A generic micromachined silicon platform for high-performance RF passive components, J. Micromech. Microeng.: Struct., Devices, Systemsdkjdot 10 (2000) 365–371.
[46] Y. Mo, Y. Okawa, K. Inoue, K. Natukawa, Low-voltage and low-power optimization of micro-heater and its on-chip drive circuitry for gas sensor array, Sens. Actuators A 100 (2002) 94–101.
[47] M.D. Steinberg, C.R. Lowe, A micropower amperometric potentiostat, Sens. Actuators B 97 (2004) 284–289.
[48] E.S. Kolesar, W.E. Odom, J.A. Jayachandran, M.D. Ruff, S.Y. Ko, J.T. Howard, P.B. Allen, J.M. Wilken, N.C. Boydston, J.E. Bosch, R.J. Wilks, J.B. McAllister, Design and performance of an electrothermal MEMS microengine capable of bi-directional motion, Thin Solid Films 447–448 (2004) 481–488.
[49] L. Beccai, S. Roccella, A. Arena, F. Valvo, P. Valdastri, A. Menciassi, M.C. Carrozza, P. Dario, Design and fabrication of a hybrid silicon three-axial force sensor for biomechanical applications, Sens. Actuators A 120 (2) (2005) 370–382.
[50] Y. Zhang, H.H. Chen, J.B. Kuo, 0.8 V CMOS adiabatic differential switch logic circuit using bootstrap technique for low-voltage low-power VLSI, Electron. Lett. 38 (24) (2002) 1497–1499.
[51] R.G. Carvajal, J. Galan, J. Ramirez-Angulo, A. Torralba, Low-power low-voltage differential class-AB OTAs for SC circuits, Electron. Lett. 38 (22) (2002) 1304–1305.
[52] G. Gramegna, P. O'Connor, P. Rehak, S. Hart, CMOS preamplifier for low-capacitance detectors, Nuclear Instrum. Methods Phys. Res. A 390 (1997) 241–250.
[53] P. Girard, C. Landrault, P. Pravossoudovitch, D. Severac, A non-iterative gate resizing algorithm for reduction in power consumption, VLSI J. 24 (1997) 37–52.
[54] C.-H. Lin, C.W. Jen, Low power parallel Huffman decoding, Electron. Lett. 34 (3) (1998) 240–241.
[55] J. Kin, M. Gupta, W.H. Mangione-Smith, Filtering Memory References to Increase Energy Efficiency, IEEE Transact. Comput. 49 (1) (2000) 1–15.
[56] http://www.rayovac.com/products/hearing/loudnclear/consumer_info.shtml, accessed November 2004.
[57] http://www.maxell.co.jp/e/products/industrial/battery/index.html, accessed December 2004.
[58] http://www.renata.com/content/3vlithium/overview.php, accessed December 2004.
[59] http://www.greatbatch.com/eps/products/ps/lowrate/default.asp, accessed December 2004.
[60] M. Jain, G. Nagasubramanian, R.G. Jungst, J.W. Weidner, Analysis of a lithium/thionyl chloride battery under moderate-rate discharge, J. Electrochem. Soc. 146 (11) (1999) 4023–4030.
[61] http://www.energizer.com, accessed June 2005.
[62] K.D. Wise, D.J. Anderson, J.F. Hetke, D.R. Kipke, K. Najafi, Wireless implantable microsystems: high-density electronic interfaces to the nervous system, in: Proceedings of the IEEE, vol. 92 (1), 2004, pp. 76–97.
[63] P. Bhatti, K.D. Wise, Personal conversation (2004).
[64] http://www.maxell.com, accessed August 2005.
[65] H.T. Liu, X. Xi, Z.P. Guo, A novel silver oxide electrode and its charge-discharge performance, J. Appl. Electrochem. 32 (2002) 275–279.
[66] A.P. Karpinski, S.J. Russell, J.R. Serenyi, J.P. Murphy, Silver based batteries for high power applications, J. Power Sources 91 (2000) 77–82.
[67] D.F. Smith, G.R. Graybill, R.K. Grubbs, J.A. Gucinski, New developments in very high rate silver oxide electrodes, J. Power Sources 65 (1997) 47–52.
[68] http://www.sjm.com/resources/learnmoreabout.aspx?section=ImplantableCardioverterDefibrillatorSystem, accessed June 2005.
[69] http://www.medtronic.com/neuro/interstim/2products.html, accessed July 2005.
[70] http://www.medtronic.com/neuro/paintherapies/pain_treatment_ladder/neurostimulation/neuro_neurostimulation.html#rechargeable, accessed July 2005.
[71] http://www.medel.com/ENG/US/20_Products/000_products_overview.asp, accessed July 2005.
[72] http://www.medtronic.com/servlet/ContentServer?pagename=Medtronic/Website/StageArticle&ConditionName=Seizures+and+Fainting&Stage=Management&Article=seizfaint_art_procedure, accessed July 2005.
[73] http://www.medtronic.com/neuro/paintherapies/pain_treatment_ladder/drug_infusion/pumps_pump_sel/drug_pumps_prog_pumps.html#introduction, July 2005.
[74] http://www.ihc.com/xp/ihc/lds/aboutus/news/article23.xml, accessed June 2005.
[75] A.J. Maniglia, G. Murray, J.E. Arnold, W.H. Ko, Bioelectronic microphone options for a totally implantable hearing device for partial and total hearing loss, Otolaryngol. Clin. North Am. 34 (2) (2001) 469–480.